Accepted Manuscript

Topology optimization for concurrent design of structures with multi-patch microstructures by level sets

Hao Li, Zhen Luo, Liang Gao, Qinghua Qin

PII: S0045-7825(17)30751-X
DOI: https://doi.org/10.1016/j.cma.2017.11.033
Reference: CMA 11692

To appear in: *Comput. Methods Appl. Mech. Engrg.*

Received date : 31 July 2017
Revised date : 23 November 2017
Accepted date : 30 November 2017

Please cite this article as: H. Li, Z. Luo, L. Gao, Q. Qin, Topology optimization for concurrent design of structures with multi-patch microstructures by level sets, *Comput. Methods Appl. Mech. Engrg.* (2017), https://doi.org/10.1016/j.cma.2017.11.033

Topology optimization for concurrent design of structures with multi-patch microstructures by level sets

Hao Li [a], Zhen Luo [b,*], Liang Gao [a,] and Qinghua Qin [c]**

[a] *The State Key Lab of Digital Manufacturing Equipment and Technology*
Huazhong University of Science and Technology, 1037 Luoyu Road, Wuhan, Hubei 430074, China

[b] *The School of Mechanical and Mechatronic Engineering*
University of Technology, Sydney, 15 Broadway, Ultimo, NSW 2007 Australia

[c] *The Research School of Engineering*
Australian National University, Acton, ACT 2601, Australia

Corresponding author: *Phone: +61 2 9514 2994; E-mail: zhen.luo@uts.edu.au (Dr Z. Luo[*])*

Phone: +86 27 8755 9419; E-mail: gaoliang@hust.edu.cn (Prof L. Gao[**])

Abstract

This paper focuses on the novel concurrent design for cellular structures consisting of multiple patches of material microstructures using a level set-based topological shape optimization method. The macro structure is featured with the configuration of a cluster of non-uniformly distributed patches, while each patch hosts a number of identical material microstructures. At macro scale, a discrete element density based approach is presented to generate an overall structural layout involving different groups of discrete element densities. At micro scale, each macro element is regarded as an individual microstructure with a discrete intermediate density. Hence, all the macro elements with the same discrete densities (volume fractions) are represented by a unique microstructure. The representative microstructures corresponding to different density groups are topologically optimized by incorporating the numerical homogenization approach into a parametric level set method. The multiscale concurrent designs are integrated into a uniform optimization procedure, so as to optimize both topologies for the macrostructure and its microstructures, as well as locations of the microstructures in the design space. Numerical examples demonstrate that the proposed method can substantially improve the structural performance with an affordable computation and manufacturing cost.

Keywords: Topology optimization; Cellular structures; Multiscale design; Level set method.

1. Introduction

Cellular solids are a kind of low density and high strength porous materials that are artificially engineered to have multifunctional properties [1-3], such as lightweight but superior structural performance in mission-critical applications. In particular, cellular structures hosting arrays of periodic microstructures with ordinary material constituents have gained considerable attention due to their flexibility in catering for a wide range of applications [2, 3]. The properties of such porous materials mainly depend on the configurations of microstructures, so the multi-functionalities of cellular structures are determined by the geometry of their microstructures rather than the intrinsic material compositions. However, it can be found that the majority of the current studies focus on the design of microscopic structures, rather than the concurrent design of microscopic properties by considering macroscopic loads and boundary conditions. Actually, in engineering, it is of great importance to simultaneously consider microstructural materials, as well as the macrostructural loads and boundary conditions. Hence, an efficient computational method that can effectively implement the concurrent design of macrostructure and its material microstructures is still in demands.

Topology optimization is a growing subfield of structural optimization that is experiencing popularity [4, 5]. Topology optimization is usually formulated as a mathematical programming problem, to iteratively search for the best layout of material or geometry in a fixed reference domain for a given set of loads, boundary conditions and constraints, until the performance of the structure is optimized. Topology optimization has demonstrated its great potential for generating a range of innovative results for various structural and material design problems, including the periodic cellular materials. Many methods have been developed for topology optimization, e.g. the homogenization method [6, 7], solid isotropic material with penalization (SIMP) [8-10], evolutionary structural optimization (ESO) [11] and level set method (LSM) [12-15].

LSM [12, 13] has been emerged as an alternative approach for structural optimization [14-24] based on the implicit representation of the boundary. In LSMs, the boundary of a structure is represented implicitly as the zero level set of a higher dimensional level set function. Then, the topology and shape changes of the boundary are mathematically governed by solving the Hamilton-Jacobi partial differential equation (H-J PDE) via appropriate numerical schemes [13-15]. However, the most conventional LSM-based topological optimization requires an elaborate implementation of finite difference schemes, so as to well settle some

typical numerical issues, e.g. Courant-Friedrichs-Lewy (CFL) condition, re-initializations and boundary velocity extensions [13-15, 22]. Furthermore, many well-established structural optimization algorithms, e.g. the optimality criteria (OC) and mathematical programming methods [8, 25] are difficult to directly apply. To tackle above issues, many alternative LSMs have been developed [17-19, 22, 23] including the parametric level set method (PLSM) [26, 27]. The core concept of the PLSM is to interpolate the original level set function using a set of radial basis functions (RBFs) [28]. Then the topological optimization problem is transformed into a relatively easier "size" optimization problem with a system of algebraic equations. The PLSM inherits the unique features of standard LSMs, while avoids their numerical difficulties in structural topology optimization. Particularly it allows the application of many more efficient optimization algorithms based on mathematical programming and etc. PLSM has been recently applied to different topology optimization problems [29-31], such as designs with multi-materials, elastic metamaterials and cellular composites. It has also been improved to cater for three-dimensional problems [32] and robust topology optimization problems [33].

Topology optimization has been applied to a wide range of design problems, including the studies both on the macro structural and microstructural designs [4, 5]. Having regard to the design of microstructures and relevant composites, Sigmund [34] proposed an inverse homogenization method to design microstructural materials with either the prescribed properties [34] or extreme properties [35]. After that, a number of cellular solids with periodic microstructures for achieving various properties, e.g. extremal thermal expansion [38], negative Poisson's ratio [29, 39], strain density [40], multiphysics and multifunctional properties [41, 42], and functionally graded properties [43-45], have been created by topology optimization with homogenization methods [34-37].

It is noted that the majority of the above studies on topology optimization focus on the single scale. However, in practice, it is also important to concurrently consider both macro and micro scales in topological designs [46]. Generally, the concurrent topology optimization aims to achieve the topologically optimized designs with a simultaneous consideration for both the microstructures and the loading and boundary conditions of the host macro structure. One typical assumption for concurrent topology optimization designs is that the periodic microstructures are identical throughout the whole macrostructure [47-54]. For example, Fujii et al. [47]

studied the topology optimization of compliance minimization problem by optimizing a uniform material microstructure for a fixed shape and topology of the macrostructure. Liu et al. [48] developed a topology optimization method for concurrent design, so as to realize the simultaneous changes of topologies for both the macrostructure and its uniformly distributed microstructures. With a similar design framework, the concurrent topology optimization has also been extended into design problems like multi-objective optimization [50, 51, 54], dynamic optimization [53] and uncertainty optimization [52]. It is easy to understand that a structure with identical microstructures can greatly facilitate the fabrication and reduce the computational cost. However, such assumption may compromise the ultimate motivation for optimizing the concerned structural performance.

Another typical assumption for the concurrent topological designs is to simultaneously optimize the overall topology of the macrostructure and the spatially-varying microstructures. The material microstructures can be tailored from element to element throughout the whole design domain of the macro structure. For example, Rodrigues and his co-workers [55, 56] proposed a hierarchical optimization method to simultaneously determine the topology of the macro structure and the material mechanical property for each microstructure. Zhang and Sun [57] developed the design element (DE) approach that combined the structural optimization with multilayered material microstructures. Schury et al. [58] investigated the free material optimization, and obtained the optimal design consisting of a number of structurally graded materials. Xia and Breitkopf [59] concurrently optimized the structure and material microstructures under the nonlinear multiscale analysis, with element-wise material microstructures. Sivapuram et al. [60] developed a topology optimization method for concurrent design of the macrostructure which hosts different microstructures, where the positions of all microstructures were predefined and fixed during the optimization. It can be found that in most of the above concurrent designs the microstructures varied from element to element in the whole design domain of the macrostructure. Such assumption for concurrent designs produces a considerable number of microstructures to be topologically optimized, which is challenging for both computation and manufacturing.

From the viewpoint of computational designs, the topological optimization for multiscale concurrent design should be able to simultaneously address the performance, computational efficiency and manufacturability of the topologically optimized structures. The different kinds and numbers of the microstructures to be designed

should be appropriately determined in the optimization. Hence, the main motivation of this paper is to develop a topology optimization method for novel concurrent design of cellular structures, with controllable kinds of microstructures over the whole macro structure, so as to reasonably expand the design space for the concurrent design with a computationally affordable cost. Firstly, a discrete element density based approach is proposed to optimize the macrostructure, in which the design variables (the densities of the macro elements) are assumed to have a number of discrete values via a threshold scheme. At each iteration, the design variables are regarded as the volume fraction constraints of the microstructural designs. Then, at the microscale, only a given number of representative microstructures are required to be topologically optimized by incorporating the PLSM with the numerical homogenization method. In this way the topology of the macrostructure, as well as the geometries and distributions of microstructures are simultaneously optimized.

2. Concurrent topology optimization with multi-patch microstructures

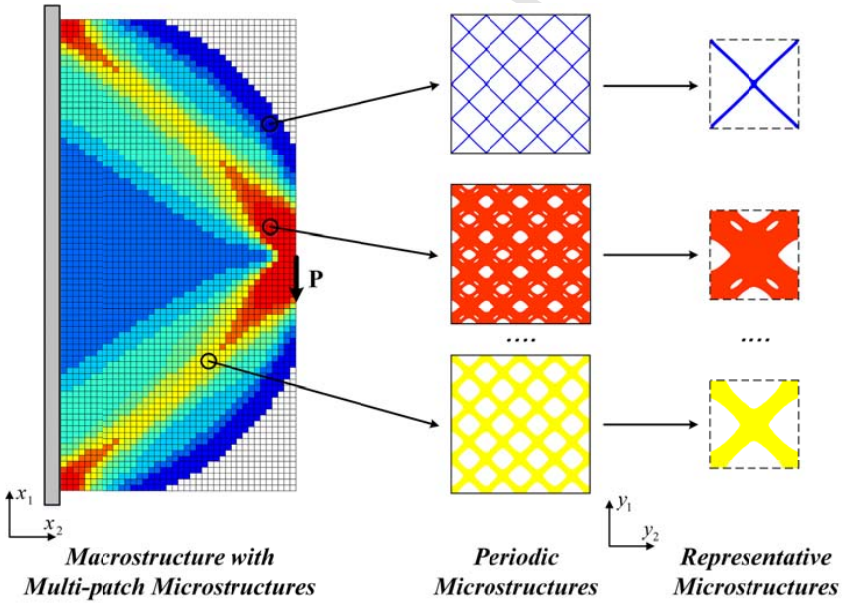

Fig. 1. Concurrent design with multi-patch microstructures

As indicated in Fig 1, the concurrent topological design involves a multiscale procedure, in which the macro and micro structural optimizations are solved simultaneously to generate a certain number of multi-patch microstructures over the entire design domain of the macrostructure. It can be seen that the current method is distinguished from the methods with microstructures varying element-to-element within the design domain, as the proposed method only optimizes a representative microstructure for a family of microstructures having the

same volume fractions. This will globally benefit the improvement of the macrostructural performance, and the computational cost of the multiscale optimization can also be greatly reduced.

Here the 'concurrent' design refers to simultaneously optimize the topology of the macrostructure, as well as configurations and distributions of microstructures in the multiscale design process. The finite element (FE) methods are applied to solve the strains at different length scales. The multiscale topology optimization aims to minimize the compliance of the macrostructure, using different types of topology optimization methods and design variables at different scales. At the macro scale, a discrete element density-based method is used to optimize the topology of the macrostructure with a given set of discrete density variables subject to a global volume constraint. At the micro scale, one macro finite element can be regarded as one microstructure with the corresponding element density, and the microstructures with the same density (or volume fraction) are grouped as one identical family of representative microstructure. Each representative microstructure is topologically optimized by using the PLSM in association with the numerical homogenization method. The concurrent design can be obtained by assembling the different families of microstructures according to their density distributions at macro scale. In the following, to facilitate the discussion, the superscripts '*MA*' and '*MI*' are used to denote the physical quantities at the macro and micro scales, respectively.

2.1 PLSM for microstructural topology optimization

In the design, the PLSM is employed at the micro scale. The first concept in the PLSM is to implicitly represent the design boundary of the structure as the zero level set of a higher dimensional level set function (LSF) with Lipschitz continuity. Assuming $\mathrm{D}^{MI} \subset \mathbb{R}^d \ (d = 2,3)$ is the fixed Eulerian reference domain containing all admissible shapes Ω^{MI}, the different phases can be represented by using the level set function ϕ^{MI} as:

$$\begin{cases} \phi^{MI}(x) > 0 & \forall x \in \Omega^{MI} \backslash \partial\Omega^{MI} \quad \text{(Solid)} \\ \phi^{MI}(x) = 0 & \forall x \in \partial\Omega^{MI} \cap \mathrm{D}^{MI} \quad \text{(Boundary)} \\ \phi^{MI}(x) < 0 & \forall x \in \mathrm{D}^{MI} \backslash \Omega^{MI} \quad \text{(Void)} \end{cases} \tag{1}$$

By introducing the pseudo-time *t*, the motion of the structural design boundary towards its optimum is actually equivalent to solving the first-order H-J PDE [12, 13]:

$$\frac{\partial \phi^{MI}(x,t)}{\partial t} - \theta^{MI}\left|\nabla \phi^{MI}(x,t)\right| = 0 \tag{2}$$

where x is the spatial variable and t is the temporal variable, and θ^{MI} is the normal velocity field [14, 15].

To eliminate the numerical difficulties [12, 13] associated with directly solving the H-J PDE, we introduce the GSRBFs (globally supported RBFs) [28], such as the Gaussian RBFs, to interpolate the LSF, as follows:

$$\phi^{MI}(x,t) = \varphi^{MI}(x)\cdot\alpha^{MI}(t) = \sum_{n=1}^{N}\varphi_n^{MI}(x)\cdot\alpha_n^{MI}(t) \tag{3}$$

where $\varphi^{MI} = \left[\varphi_1^{MI}, \varphi_2^{MI}, ..., \varphi_N^{MI}\right]$ are the RBFs, and $\alpha^{MI} = \left[\alpha_1^{MI}, \alpha_2^{MI}, ..., \alpha_N^{MI}\right]^{\mathrm{T}}$ is the vector including the generalized expansion coefficients. N is the number of RBF knots. The Gaussian RBFs are known as a kind of widely accepted RBFs with global supports [26, 28]:

$$\varphi_n^{MI}(x) = e^{-cr_n(x)^2} \quad (n = 1, 2, \ldots, N) \tag{4}$$

where r defined in a Euclidean space can be expressed by:

$$r(x) = \left\|x - x_I\right\| \tag{5}$$

where x_I is the coordinate of knot I. c is the shape parameter that is equal to the physical size of a level set grid [26, 28]. It is noted that the CSRBFs (compactly supported RBFs) [27, 28] may lose accuracy in the numerical interpolation, particularly when the microstructural design is subject to a relatively small volume constraint. The GSRBF can guarantee the numerical accuracy, but its full interpolation matrix will substantially increase the computational cost. Hence, a matrix compression scheme, e.g. the discrete wavelet transform [32, 61], can be used to compress the full matrix of the GSRBF to reduce the interpolation cost while keep a very good numerical accuracy. The compression of the interpolation matrix is beyond the scope of this study, the readers can refer to [32, 61] for more related details.

By substituting Eq. (3) into Eq. (2), the H-J PDE is changed into a system of ordinary differential equations:

$$\varphi^{MI}(x)\frac{d\alpha^{MI}(t)}{dt} - \theta^{MI}\left|\nabla \varphi^{MI}(x)\alpha^{MI}(t)\right| = 0 \tag{6}$$

Then the normal velocity field can be given by

$$\theta^{MI} = \frac{\varphi^{MI}(x)}{\left|\nabla\varphi^{MI}(x)\alpha^{MI}(t)\right|}\dot{\alpha}^{MI}(t), \text{ where } \dot{\alpha}^{MI}(t) = \frac{d\alpha^{MI}(t)}{dt} \tag{7}$$

It is noted that the design variables in PLSM are recognized as the expansion coefficients α^{MI} rather than the LSF ϕ^{MI}. The PLSM can be easily implemented and has been applied to different topology optimization applications [27, 29, 31-33] without experiencing the typical numerical difficulties in most conventional topology optimization methods using level sets, such as the re-initialization, velocity extension and CFL condition [14, 15]. Furthermore, many well-established structural optimization algorithms that are more efficient can be directly applied to solve the PLSM-based optimization model.

2.2 Numerical homogenization method

In this paper, the numerical homogenization method [34, 36] is employed to evaluate the effective material properties of the microstructures by imposing periodic boundary conditions [62]. Since the macrostructure is not fully configured with a number of identical microstructures, the periodic boundary conditions cannot be accurately met. However, as shown in [43, 44], when the variation of the property gradient between two neighboring microstructures is relatively small, the numerical homogenization method can still be applied to approximate the effective properties of the microstructure.

Based on the asymptotic approximation, the effective elastic tensor for each element can be calculated by

$$D_{ijkl}^{H}\left(u^{MI},\phi^{MI}\right) = \frac{1}{\left|\Omega^{MI}\right|}\int_{\Omega^{MI}}\left(\varepsilon_{pq}^{0(ij)} - \varepsilon_{pq}^{*}\left(u^{MI(ij)}\right)\right)D_{pqrs}\left(\varepsilon_{rs}^{0(kl)} - \varepsilon_{rs}^{*}\left(u^{MI(kl)}\right)\right)H\left(\phi^{MI}\right)d\Omega^{MI} \tag{8}$$

where $i,j,k,l = 1,2,\ldots,d$, and d is the spatial dimension. $H(\cdot)$ denotes the Heaviside function which serves as a characteristic function to indicate different parts of the design domain [14, 15]. More details regarding the Heaviside function can be found in Section 4. Ω^{MI} is the domain of the microstructure, and $\left|\Omega^{MI}\right|$ is the area or volume of the microstructure. $\varepsilon_{pq}^{0(ij)}$ denote the macroscopic unit strains including three components in two-dimensional (2D) and six components in three-dimensional (3D) cases [34, 36]. $\varepsilon_{pq}^{*}\left(u^{MI(ij)}\right)$ are locally varying strain fields induced by $\varepsilon_{pq}^{0(ij)}$. D_{pqrs} is the elasticity tensor of a solid material.

The displacement $u^{MI(ij)}$ corresponding to $\varepsilon_{pq}^{*}\left(u^{MI(ij)}\right)$ can be calculated by solving the following equations

with the given macroscopic strain $\varepsilon_{pq}^{0(ij)}$:

$$\int_{\Omega^{MI}} \left(\varepsilon_{pq}^{0(ij)} - \varepsilon_{pq}^{*} \left(u^{MI(ij)} \right) \right) D_{pqrs} \varepsilon_{rs}^{*} \left(v^{MI(ij)} \right) H\left(\phi^{MI} \right) d\Omega^{MI} = 0, \ \forall v^{MI(ij)} \in \bar{\mathrm{U}}\left(\Omega^{MI} \right) \tag{9}$$

where $v^{MI(ij)}$ are the virtual displacement fields in the microstructure. $\bar{\mathrm{U}}\left(\Omega^{MI}\right)$ indicates the kinematically admissible displacement field under the periodic boundary conditions. For each representative microstructure subject to the given macroscopic strain fields, Eq. (9) can be solved via the finite element method to obtain the displacements $u^{MI(ij)}$, and then the displacement fields $u^{MI(ij)}$ can be further substituted into Eq. (8) to calculate the effective elastic tensor D_{ijkl}^{H} for each microstructure at macroscopic scale.

2.3 Discrete density based method for macrostructural optimization

In the discrete density based method, the pseudo density ρ of each macro element is regarded as the design variable, which is similar to that in the standard SIMP approach [8, 9]. The density '0' of an element means void, and the density '1' indicates solid, while the density (0, 1) represents intermediate density. Then, the elasticity tensor $D^{MA}\left(\rho_e^{MA}\right)$ can be interpolated by:

$$D_{ijkl}^{MA}\left(\rho_e^{MA}\right) = \rho_e^{MA} \cdot \left(\tilde{D}_e^{0}\right)_{ijkl} \tag{10}$$

where e=1,2,…,E, and E denotes the total number of the macro finite elements. ρ_e^{MA} is the pseudo density of the e^{th} macro element. $\tilde{D}_e^{0}$ is a variable used to identify the equivalent base material property for the macro element e. In the current optimization method, one macro scale finite element is assumed to be equivalent to one microstructure with the same densities, which can lead to:

$$D_{ijkl}^{MA}\left(\rho_e^{MA}\right) = D_{ijkl}^{H}\left(u_e^{MI}, \phi_e^{MI}\right) \tag{11}$$

where $D^{H}\left(u_e^{MI}, \phi_e^{MI}\right)$ is the effective elasticity tensor of the macro element e, which is evaluated by Eq. (8).

According to Eqs. (10) and (11), $\tilde{D}_e^{0}$ can be given by:

$$\left(\tilde{D}_e^{0}\right)_{ijkl} = D_{ijkl}^{H}\left(u_e^{MI}, \phi_e^{MI}\right) \Big/ \rho_e^{MA} \tag{12}$$

In this study, $\tilde{D}_e^{0}$ is no longer the natural property of the solid material e, and it actually acts as a temporal value varying in the optimization. Before macrostructural optimization at each iteration, we first need to calculate $\tilde{D}_e^{0}$ for each microstructure by using Eq. (12). In Eq. (12), it is noted that D_{ijkl}^{H} and ρ_e^{MA} are regarded as the known values, which are predetermined by the results obtained from the previous iteration. Then, the new $\tilde{D}_e^{0}$ of each microstructure is fixed at the current iteration, and can be used in the macrostructural optimization to update ρ_e^{MA} (i.e. the macrostructural topology).

Obviously, ρ_e^{MA} can be any values between '0' and '1'. However, the discrete density-based method only allows the design variables having serval predefined values, e.g. $[\rho_0 < \rho_1 < ... < \rho_M]$. $\rho_0 = 0.001$ represents the density of a void finite element at macro scale, and $\rho_M = 1$ denotes the density of a solid finite element at macro scale. Thus, a threshold scheme is further used to convert the continuous design variables into a set of discrete variables. When a continuous design variable satisfies $\rho_{m-1} \le \rho_e^{MA} \le \rho_m \ \ (m = 1, 2, ..., M)$, its term $\tilde{\rho}_e^{MA}$ after the threshold operation can be defined by using the following heuristic scheme:

$$\tilde{\rho}_e^{MA} = \begin{cases} \rho_{m-1} & if \ \ \rho_e^{MA} - \rho_{m-1} \le \rho_m - \rho_e^{MA} \\ \rho_m & if \ \ \rho_e^{MA} - \rho_{m-1} > \rho_m - \rho_e^{MA} \end{cases} \tag{13}$$

The discrete density based method is different from the standard SIMP scheme [4, 8, 9] due to the following three aspects: (1) no penalty factor is required to suppress the elements with intermediate densities; (2) only a limited number of discrete variables can be attained from the original set of continuous design variables; (3) the equivalent base material property $\tilde{D}_e^0$ can be isotropic, orthotropic and even anisotropic.

2.4 Macrostructural topology optimization

At the macro scale, the compliance topology optimization problem can be stated as:

$$\begin{aligned} &Find \quad \rho_e^{MA} \ \ (e = 1, 2, ..., E) \\ &Min \quad F\left(\rho^{MA}\right) = \int_{\Omega^{MA}} \varepsilon_{ij}\left(u^{MA}\right) D_{ijkl}^{MA}\left(\rho^{MA}\right) \varepsilon_{kl}\left(u^{MA}\right) d\Omega^{MA} \\ &S.t. \quad G\left(\rho^{MA}\right) = \int_{\Omega^{MA}} \rho^{MA} V_0^{MA} d\Omega^{MA} - V_{\max} \le 0, \\ &\qquad a\left(u^{MA}, v^{MA}, \rho^{MA}\right) = l\left(v^{MA}\right) \quad \forall v^{MA} \in \bar{\mathrm{U}}\left(\Omega^{MA}\right), \\ &\qquad \rho_{\min} \le \rho_e^{MA} \le \rho_{\max}. \end{aligned} \tag{14}$$

where F is the objective function. G is the global volume constraint of the macrostructure, and $V_{\max}$ is the corresponding material usage limitation. V_0^{MA} denotes the volume of a macro finite element with solid material. ε represents the strain field. Ω^{MA} is the macroscale design domain. u^{MA} is the macro displacement, v^{MA} is the virtual displacement at macro scale and belongs to the kinematically admissible displacement field $\bar{\mathrm{U}}\left(\Omega^{MA}\right)$. $\rho_{\min} = 0.001$ and $\rho_{\max} = 1$ are the lower and upper bounds of the macro design variables, respectively. The functionals used in the macro FE analysis are respectively given as:

$$a(u^{MA}, v^{MA}, \rho^{MA}) = \int_{\Omega^{MA}} \varepsilon_{ij}\left(u^{MA}\right) D_{ijkl}^{MA}\left(\rho^{MA}\right) \varepsilon_{kl}\left(v^{MA}\right) d\Omega^{MA} \tag{15}$$

$$l\left(v^{MA}\right) = \int_{\Omega^{MA}} f v^{MA} d\Omega^{MA} + \int_{\partial\Omega^{MA}} \tau v^{MA} d\Gamma^{MA} \tag{16}$$

where f is the body force, and τ is the traction along the boundary Γ^{MA}. It is noted that the heuristic scheme given in (13) is applied to all the continuous design variables ρ_e^{MA} at each iteration, so as to achieve a given set of discrete design variables $\tilde{\rho}_e^{MA}=\rho_m \ \ (m=0,1,...,M)$.

2.5 Microstructural topology optimization

At each iteration, the discrete macroscale densities are regarded as the maximum material volume fractions for the representative microstructures. Meanwhile, the distributions of microstructures under different volume fractions also correspond to the distributions of finite element densities at macro scale. Hence, the micro scale topology optimization problem can be established by

$$\begin{aligned} &Find \quad \alpha_{m,n}^{MI} \ \ (m=0,1,...,M;n=1,2,...,N) \\ &Min \quad F\left(\alpha^{MI}\right)=\int_{\Omega^{MA}} \varepsilon_{ij}\left(u^{MA}\right) D_{ijkl}^{H}\left(u^{MI},\phi^{MI}\left(\alpha^{MI}\right)\right)\varepsilon_{kl}\left(u^{MA}\right)d\Omega^{MA} \\ &S.t. \quad G_m\left(\alpha^{MI}\right)=\int_{\Omega_m^{MI}} H\left(\phi^{MI}\left(\alpha^{MI}\right)\right)d\Omega_m^{MI}-\rho_m V_0^{MA}\le 0, \\ &\qquad a\left(u^{MA},v^{MA},u^{MI},\phi^{MI}\right)=l\left(v^{MA}\right) \ \ \forall v^{MA}\in \bar{\mathrm{U}}\left(\Omega^{MA}\right), \\ &\qquad \alpha_{\min}\le\alpha_{m,n}^{MI}\le\alpha_{\max}. \end{aligned} \tag{17}$$

where the subscripts *n* and *m* indicate the knot *n* in the micro level set grid, which belongs to the m^{th} representative microstructure. *N* is the total number of micro level set knots for a representative microstructure, and *M* is the number to denote different types of representative microstructures. Ω_m^{MI} is the design domain of the m^{th} representative microstructure. G_m is the local volume constraint for the m^{th} microstructure, subject to the maximal volume fraction of $\rho_m \ \ (\rho_0<...<\rho_M)$, which is actually the discrete design variable at the macro scale after the threshold. $\alpha_{m,n}^{MI}$ are the expansion coefficients in the Gaussian RBF interpolation, which serve as the design variables for the topology optimization at the micro scale. $\alpha_{\max}$ and $\alpha_{\min}$ are the upper and lower bounds of the micro design variables. It can be seen that there are a number of ($M-2$) different representative microstructures (excluding void and solid) to be optimized at the micro scale. In this paper, the different microstructural topology designs can be simultaneously optimized by using the parallel computing in order to improve computational efficiency. The bilinear functional defined in Eq. (15) is rewritten as:

$$a\left(u^{MA},v^{MA},u^{MI},\phi^{MI}\right)=\int_{\Omega^{MA}} \varepsilon_{ij}\left(u^{MA}\right) D_{ijkl}^{H}\left(u^{MI},\phi^{MI}\right)\varepsilon_{kl}\left(v^{MA}\right)d\Omega^{MA} \tag{18}$$

As above, the macroscale and microscale optimizations in the presented method are coupled, which are actually bridged by the homogenized elasticity tensor and the element density at the macro scale (or the

volume fraction of the microstructure). Here the global volume constraint determines the maximal material usage of the macrostructure, while the local volume constraints define the material usages of different representative microstructures.

As indicated above, the proposed method contains several merits: (1) It allows for additional constraints (e.g. manufacturing constraints) during both the macrostructure and microstructure optimizations to satisfy some special engineering requirements; (2) Since the number of different types of microstructures is controllable, the computation and manufacturing costs of the design by using proposed method can be greatly reduced, when compared to the concurrent design with microstructures varying from element to element over the macrostructure; (3) As the PLSM is used to devise the microstructures with the clear geometries, the multiscale design can facilitate the fabrication without extensive post-processing.

3. Sensitivity analysis and optimization algorithm

Since the optimality criteria (OC) method [8] is employed to update the design variables at both scales, it is necessary to calculate the first-order derivatives of the objective functions and the volume constraints.

3.1 Sensitivity analysis at macro scale

It is easy to derive the derivative of the structural compliance with respect to the macro design variables by using the adjoint variable method [63], and the sensitivity information is given by

$$\frac{\partial F\left(\rho^{MA}\right)}{\partial \rho_e^{MA}} = -\int_{\Omega_e^{MA}} \varepsilon_{ij}\left(u_e^{MA}\right)\left(\tilde{D}_e^0\right)_{ijkl} \varepsilon_{kl}\left(u_e^{MA}\right) d\Omega_e^{MA} \tag{19}$$

where Ω_e^{MA} denotes the domain of macro element *e*.

Similarly, the derivative of the volume constraint with respect to the macro design variables is obtained by:

$$\frac{\partial G\left(\rho^{MA}\right)}{\partial \rho_e^{MA}} = V_0^{MA} \tag{20}$$

3.2 Update of design variables at macro scale

After obtaining the sensitivities of the objective function as well as the volume constraint, the following OC-based heuristic scheme is used to update the macro design variables [4, 8]:

$$\rho_e^{MA(\kappa+1)}=\begin{cases}\min\left[\left(\eta^{MA}+1\right)\rho_e^{MA(\kappa)},\rho_{\max}\right], & if\ \min\left[\left(\eta^{MA}+1\right)\rho_e^{MA(\kappa)},\rho_{\max}\right]\le\left[B_e^{MA(\kappa)}\right]^{\zeta^{MA}}\rho_e^{MA(\kappa)}\\ \left[B_e^{MA(\kappa)}\right]^{\zeta^{MA}}\rho_e^{MA(\kappa)}, & if\ \begin{cases}\max\left[\left(1-\eta^{MA}\right)\rho_e^{MA(\kappa)},\rho_{\min}\right]<\left[B_e^{MA(\kappa)}\right]^{\zeta^{MA}}\rho_e^{MA(\kappa)}\\ \left[B_e^{MA(\kappa)}\right]^{\zeta^{MA}}\rho_e^{MA(\kappa)}<\min\left[\left(\eta^{MA}+1\right)\rho_e^{MA(\kappa)},\rho_{\max}\right]\end{cases}\\ \max\left[\left(1-\eta^{MA}\right)\rho_e^{MA(\kappa)},\rho_{\min}\right], & if\ \left[B_e^{MA(\kappa)}\right]^{\zeta^{MA}}\rho_e^{MA(\kappa)}\le\max\left[\left(1-\eta^{MA}\right)\rho_e^{MA(\kappa)},\rho_{\min}\right]\end{cases}\tag{21}$$

where κ denotes the iteration number. As denoted in the standard OC method [4, 8], $\eta^{MA}\left(0<\eta^{MA}<1\right)$ is the moving limit, and $\zeta^{MA}\left(0<\zeta^{MA}<1\right)$ is the damping coefficient. B_e^{MA} can be expressed based on the optimality condition and the sensitivity information:

$$B_e^{MA(\kappa)}=-\frac{\partial F\left(\rho^{MA}\right)}{\partial\rho_e^{MA(\kappa)}}\Big/\Lambda^{MA(\kappa)}\frac{\partial G\left(\rho^{MA}\right)}{\partial\rho_e^{MA(\kappa)}}\tag{22}$$

where Λ^{MA} is the Lagrangian multiplier that can be found by a bi-sectioning algorithm [4]. Since the OC method can only deal with the continuous design variables, the design variables updated by Eq. (21) will be further regularized with Eq. (13), so as to let the design variables after thresholding have discrete values.

3.3 Sensitivity analysis at micro scale

Here, the shape derivative [63, 64] is introduced to compute the design sensitivity of the microstructure represented by the level sets [14, 15]. The shape derivatives of $F\left(\alpha^{MI}\right)$, $a\left(u^{MA},v^{MA},u^{MI},\phi^{MI}\right)$ and $l\left(v^{MA}\right)$ can be respectively expressed as follows:

$$\frac{\partial F\left(\alpha^{MI}\right)}{\partial t}=\int_{\Omega^{MA}}\left[2\varepsilon_{ij}\left(\dot{u}^{MA}\right)D_{ijkl}^{H}\left(u^{MI},\phi^{MI}\right)\varepsilon_{kl}\left(u^{MA}\right)+\varepsilon_{ij}\left(u^{MA}\right)\frac{\partial D_{ijkl}^{H}\left(u^{MI},\phi^{MI}\right)}{\partial t}\varepsilon_{kl}\left(u^{MA}\right)\right]d\Omega^{MA}\tag{23}$$

$$\begin{aligned}\frac{\partial a}{\partial t}=&\int_{\Omega^{MA}}\left[\varepsilon_{ij}\left(\dot{u}^{MA}\right)D_{ijkl}^{H}\left(u^{MI},\phi^{MI}\right)\varepsilon_{kl}\left(v^{MA}\right)+\varepsilon_{ij}\left(u^{MA}\right)D_{ijkl}^{H}\left(u^{MI},\phi^{MI}\right)\varepsilon_{kl}\left(\dot{v}^{MA}\right)\right]d\Omega^{MA}\\&+\int_{\Omega^{MA}}\varepsilon_{ij}\left(u^{MA}\right)\frac{\partial D_{ijkl}^{H}\left(u^{MI},\phi^{MI}\right)}{\partial t}\varepsilon_{kl}\left(v^{MA}\right)d\Omega^{MA}\end{aligned}\tag{24}$$

$$\frac{\partial l}{\partial t}=\int_{\Omega^{MA}}f\dot{v}^{MA}d\Omega^{MA}+\int_{\partial\Omega^{MA}}\tau\dot{v}^{MA}d\Gamma^{MA}\tag{25}$$

Considering the terms containing $\dot{v}^{MA}$ in Eqs. (24) and (25), we can establish the following equation

$$\int_{\Omega^{MA}}\varepsilon_{ij}\left(u^{MA}\right)D_{ijkl}^{H}\left(u^{MI},\phi^{MI}\right)\varepsilon_{kl}\left(\dot{v}^{MA}\right)d\Omega^{MA}=\int_{\Omega^{MA}}f\dot{v}^{MA}d\Omega^{MA}+\int_{\partial\Omega^{MA}}\tau\dot{v}^{MA}d\Gamma^{MA}\tag{26}$$

Meanwhile, differentiating the equilibrium equation at macro scale with respect to *t* yields:

$$\frac{\partial a\left(u^{MA},v^{MA},u^{MI},\phi^{MI}\right)}{\partial t}=\frac{\partial l\left(v^{MA}\right)}{\partial t} \tag{27}$$

Substituting Eqs. (24)-(26) into Eq. (27) yields:

$$\int_{\Omega^{MA}}\varepsilon_{ij}\left(\dot{u}^{MA}\right)D_{ijkl}^{H}\left(u^{MI},\phi^{MI}\right)\varepsilon_{kl}\left(v^{MA}\right)d\Omega^{MA}=-\int_{\Omega^{MA}}\varepsilon_{ij}\left(u^{MA}\right)\frac{\partial D_{ijkl}^{H}\left(u^{MI},\phi^{MI}\right)}{\partial t}\varepsilon_{kl}\left(v^{MA}\right)d\Omega^{MA} \tag{28}$$

Since the compliance optimization problem is self-adjoint [4, 14, 15], we can rewrite the shape derivative of the objective function by substituting Eq. (28) into Eq. (23):

$$\frac{\partial F\left(\alpha^{MI}\right)}{\partial t}=-\int_{\Omega^{MA}}\varepsilon_{ij}\left(u^{MA}\right)\frac{\partial D_{ijkl}^{H}\left(u^{MI},\phi^{MI}\right)}{\partial t}\varepsilon_{kl}\left(u^{MA}\right)d\Omega^{MA} \tag{29}$$

Based on [29, 30], the derivative of the effective elasticity tensor with respect to t can be obtained by:

$$\frac{\partial D_{ijkl}^{H}\left(u_m^{MI},\phi_m^{MI}\right)}{\partial t}=-\frac{1}{\left|\Omega_m^{MI}\right|}\int_{\Omega_m^{MI}}\beta\left(u_m^{MI}\right)\theta_m^{MI}\left|\nabla\phi_m^{MI}\right|\delta\left(\phi_m^{MI}\right)d\Omega_m^{MI} \tag{30}$$

where $\delta(\cdot)$ is the derivative of the Heaviside function [14, 15]. θ_m^{MI} is the normal velocity within the design domain of m^{th} representative microstructure. The term $\beta\left(u_m^{MI}\right)$ is expressed by:

$$\beta\left(u_m^{MI}\right)=\left(\varepsilon_{pq}^{0(ij)}-\varepsilon_{pq}^{*}\left(u_m^{MI(ij)}\right)\right)D_{pqrs}\left(\varepsilon_{rs}^{0(kl)}-\varepsilon_{rs}^{*}\left(u_m^{MI(kl)}\right)\right) \tag{31}$$

By substituting the normal velocity θ_m^{MI} defined in Eq. (7) into Eq. (30), we have:

$$\frac{\partial D_{ijkl}^{H}\left(u_m^{MI},\phi_m^{MI}\right)}{\partial t}=-\sum_{n=1}^{N}\left(\frac{1}{\left|\Omega_m^{MI}\right|}\int_{\Omega_m^{MI}}\beta\left(u_m^{MI}\right)\varphi_{m,n}^{MI}\left(x\right)\delta\left(\phi_m^{MI}\right)d\Omega_m^{MI}\right)\cdot\frac{\partial\alpha_{m,n}^{MI}}{\partial t} \tag{32}$$

According to the chain rule, the derivative of the effective elasticity tensor with respect to t is

$$\frac{\partial D_{ijkl}^{H}\left(u_m^{MI},\phi_m^{MI}\right)}{\partial t}=\sum_{n=1}^{N}\frac{\partial D_{ijkl}^{H}\left(u_m^{MI},\phi_m^{MI}\right)}{\partial\alpha_{m,n}^{MI}}\cdot\frac{\partial\alpha_{m,n}^{MI}}{\partial t} \tag{33}$$

By comparing the corresponding terms in Eq. (32) and Eq. (33), we can find the derivative of effective property tensor with respect to the design variables

$$\frac{\partial D_{ijkl}^{H}\left(u_m^{MI},\phi_m^{MI}\right)}{\partial\alpha_{m,n}^{MI}}=-\frac{1}{\left|\Omega_m^{MI}\right|}\int_{\Omega_m^{MI}}\beta\left(u_m^{MI}\right)\varphi_{m,n}^{MI}\left(x\right)\delta\left(\phi_m^{MI}\right)d\Omega_m^{MI} \tag{34}$$

Recalling Eq. (29) and substituting Eq. (33) into Eq. (29), it yields:

$$\frac{\partial F\left(\alpha^{MI}\right)}{\partial t}=-\sum_{m=1}^{M}\int_{\Omega_m^{MA}}\varepsilon_{ij}\left(u_m^{MA}\right)\left[\sum_{n=1}^{N}\frac{\partial D_{ijkl}^{H}\left(u_m^{MI},\phi_m^{MI}\right)}{\partial\alpha_{m,n}^{MI}}\cdot\frac{\partial\alpha_{m,n}^{MI}}{\partial t}\right]\varepsilon_{kl}\left(u_m^{MA}\right)d\Omega_m^{MA} \tag{35}$$

On the other hand, the derivative of $F\left(\alpha^{MI}\right)$ with respect to *t* can be calculated by using the chain rule as:

$$\frac{\partial F\left(\alpha^{MI}\right)}{\partial t}=\sum_{m=1}^{M}\sum_{n=1}^{N}\frac{\partial F\left(\alpha^{MI}\right)}{\partial\alpha_{m,n}^{MI}}\cdot\frac{\partial\alpha_{m,n}^{MI}}{\partial t} \tag{36}$$

Again, comparing the corresponding terms in Eq. (35) and Eq. (36), the derivative of $F\left(\alpha^{MI}\right)$ with respect to the design variables can be obtained by:

$$\frac{\partial F\left(\alpha^{MI}\right)}{\partial\alpha_{m,n}^{MI}}=-\int_{\Omega_m^{MA}}\varepsilon_{ij}\left(u_m^{MA}\right)\left(\frac{\partial D_{ijkl}^{H}\left(u_m^{MI},\phi_m^{MI}\right)}{\partial\alpha_{m,n}^{MI}}\right)\varepsilon_{kl}\left(u_m^{MA}\right)d\Omega_m^{MA} \tag{37}$$

Similarly, the derivatives of the local volume constraints associated with the design variables are derived:

$$\frac{\partial G_m\left(\alpha^{MI}\right)}{\partial\alpha_{m,n}^{MI}}=\int_{\Omega_m^{MI}}\varphi_{m,n}^{MI}\left(x\right)\delta\left(\phi_m^{MI}\right)d\Omega_m^{MI} \tag{38}$$

3.4 Update of design variables at micro scale

At the micro scale, an OC-based algorithm is also used to update the micro design variables. Similarly, a heuristic updating scheme is established based on the Kuhn-Tucker conditions [4]:

$$\tilde{\alpha}_{m,n}^{MI(\kappa+1)}=\begin{cases}\min\left[\left(\eta^{MI}+1\right)\tilde{\alpha}_{m,n}^{MI(\kappa)},\tilde{\alpha}_{m,\max}^{MI}\right], & if\ \min\left[\left(\eta^{MI}+1\right)\tilde{\alpha}_{m,n}^{MI(\kappa)},\tilde{\alpha}_{m,\max}^{MI}\right]\le\left[B_{m,n}^{MI(\kappa)}\right]^{\zeta^{MI}}\tilde{\alpha}_{m,n}^{MI(\kappa)}\\ \left[B_{m,n}^{MI(\kappa)}\right]^{\zeta^{MI}}\tilde{\alpha}_{m,n}^{MI(\kappa)}, & if\begin{cases}\max\left[\left(1-\eta^{MI}\right)\tilde{\alpha}_{m,n}^{MI(\kappa)},\tilde{\alpha}_{m,\min}^{MI}\right]<\left[B_{m,n}^{MI(\kappa)}\right]^{\zeta^{MI}}\tilde{\alpha}_{m,n}^{MI(\kappa)}\\ \left[B_{m,n}^{MI(\kappa)}\right]^{\zeta^{MI}}\tilde{\alpha}_{m,n}^{MI(\kappa)}<\min\left[\left(\eta^{MI}+1\right)\tilde{\alpha}_{m,n}^{MI(\kappa)},\tilde{\alpha}_{m,\max}^{MI}\right]\end{cases}\\ \max\left[\left(1-\eta^{MI}\right)\tilde{\alpha}_{m,n}^{MI(\kappa)},\tilde{\alpha}_{m,\min}^{MI}\right], & if\ \left[B_{m,n}^{MI(\kappa)}\right]^{\zeta^{MI}}\tilde{\alpha}_{m,n}^{MI(\kappa)}\le\max\left[\left(1-\eta^{MI}\right)\tilde{\alpha}_{m,n}^{MI(\kappa)},\tilde{\alpha}_{m,\min}^{MI}\right]\end{cases} \tag{39}$$

where the moving limit $\eta^{MI}\left(0<\eta^{MI}<1\right)$ and the damping parameter $\zeta^{MI}\left(0<\zeta^{MI}<1\right)$ are introduced to stabilize the iterative process. $B_{m,n}^{MI(\kappa)}$ can be defined by:

$$B_{m,n}^{MI(\kappa)}=-\frac{\partial F\left(\alpha^{MI}\right)}{\partial\alpha_{m,n}^{MI(\kappa)}}\Bigg/\max\left(\vartheta,\Lambda_m^{MI(\kappa)}\frac{\partial G_m\left(\alpha^{MI}\right)}{\partial\alpha_{m,n}^{MI(\kappa)}}\right) \tag{40}$$

where ϑ is a small positive constant to avoid zero terms, and the Lagrangian multiplier Λ_m^{MI} can also be updated by the bi-sectioning algorithm [4]. The lateral bounds are $\tilde{\alpha}_{m,\min}^{MI}$=0.001 and $\tilde{\alpha}_{m,\max}^{MI}$=1. To facilitate the numerical implementation, $\tilde{\alpha}_{m,n}^{MI}$ is regarded as a regularized form of the actual design variable $\alpha_{m,n}^{MI}$:

$$\tilde{\alpha}_{m,n}^{MI(\kappa)}=\frac{\alpha_{m,n}^{MI(\kappa)}-\alpha_{m,\min}^{MI(\kappa)}}{\alpha_{m,\max}^{MI(\kappa)}-\alpha_{m,\min}^{MI(\kappa)}} \tag{41}$$

where $\alpha_{m,\min}^{MI(\kappa)}$ and $\alpha_{m,\max}^{MI(\kappa)}$ can be defined by:

$$\alpha_{m,\min}^{MI(\kappa)}=2\times\min\left(\alpha_{m,n}^{MI(\kappa)}\right),\quad \alpha_{m,\max}^{MI(\kappa)}=2\times\max\left(\alpha_{m,n}^{MI(\kappa)}\right) \tag{42}$$

4. Numerical implementation

The microscale equilibrium equation given in Eq. (9) can be solved by the FE method. However, in numerical implementation, the standard FE method may have difficulties to evaluate the strains of those elements cut by the moving boundary, because the material distribution within such elements are not uniform. In this study, the simple but widely used "ersatz material" model [15] is adopted to calculate the strains, so as to avoid the time-consuming remeshing process when the structural boundary is updated during the iteration. It assumes that the density, strain and stiffness of an element are approximately proportional to its area fraction or volume fraction, and meanwhile the voids within the design domain are filled with a kind of weak material. Thus, the Heaviside function in above equations is defined as a kind of step function [15, 27], which is also related to the element area or volume fraction. The derivative of the Heaviside step function is defined as follows:

$$\delta\left(\phi\right)=\frac{1}{\pi}\cdot\frac{\gamma}{\phi^2+\gamma^2} \tag{43}$$

where γ is selected as 2-4 times of the mesh size according to the numerical experiences.

As discussed in [43, 65, 66], it is essential to tackle the connectivity issue between the adjacent microstructures to produce a manufacturable design, when different microstructures occupy the macro design domain. In this study, the kinematically connective constraint approach [43] is used to guarantee the connectivity of neighboring microstructures. As shown in Fig. 2, a number of identical predefined connectors, which serves as the non-design components, are placed at the same positions within all the microstructures. It is noted that these connectors will more or less restrict the design freedom in the concurrent optimization, and thus they may slightly compromise the performance of the optimized design. However, in engineering it is acceptable to reasonably sacrifice structural design performance in order to facilitate manufacturability.

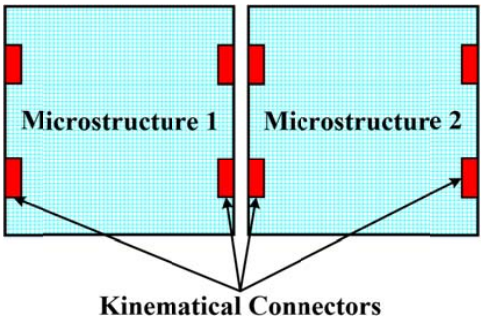

Fig. 2. Sketch for defining connectors between two adjacent microstructures

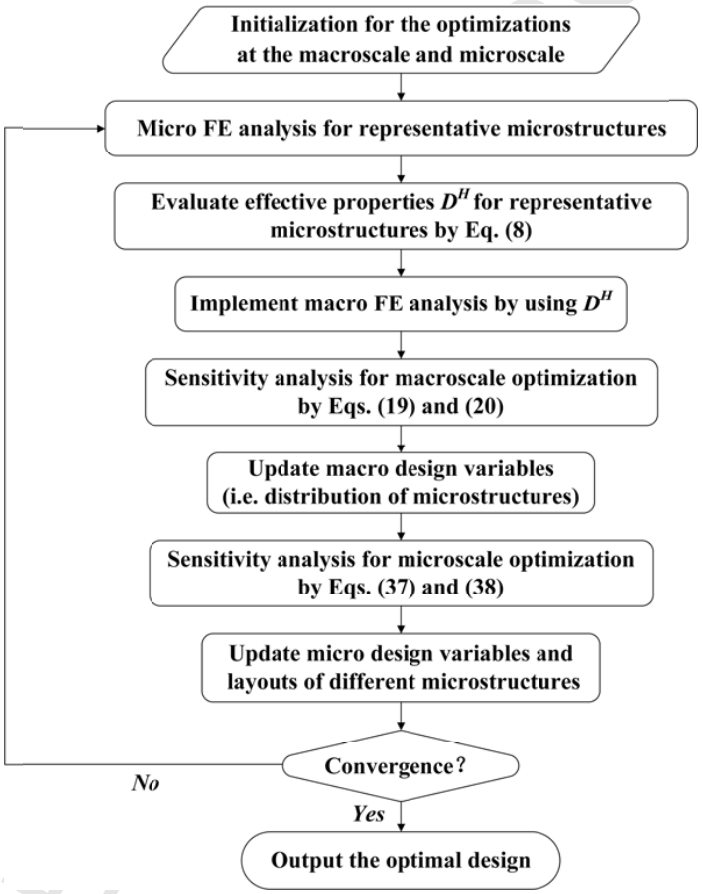

Fig. 3. Flowchart of the proposed method

Fig. 3 shows the flowchart for the numerical implementation of the proposed method. Here, the effective elasticity tensors of different microstructures are approximated by using the numerical homogenization method (Eq. (8)), with the induced displacement fields obtained by the micro FE analyses. Based on the

homogenized material properties, the macro FE analysis is implemented to calculate the macro displacement fields and the macrostructural compliance. Then, the derivatives of the objective function and the global volume constraint with respect to the macro design variables are computed by Eqs. (19) and (20). An OC algorithm given in Eq. (21) is employed to update the macro design variables and a regularizing scheme defined in Eq. (13) is then used to convert the continuous design variables into the discrete ones, so as to optimize the macrostructural topology and determine the distribution of different microstructures. After that, the sensitivity analysis is applied to all the microstructural optimizations by using Eqs. (37) and (38). Another OC algorithm given in Eq. (39) is adopted to update the micro design variables, as well as the topologies of different microstructures. The optimization process repeats until the convergent criterion is satisfied.

5. Numerical examples

In this section, several 2D and 3D numerical examples are used to illustrate the performance of the proposed concurrent design method. For the base material, its Young's modulus is E_0=10, and Poisson's ratio is μ_0=0.3. For simplicity, a finite element at the macro scale is regarded as a microstructure at the micro scale. The microstructures are discretized into 80×80=6400 elements with 4 nodes for 2D cases, and 20×20×20=8000 elements with 8 nodes for 3D cases, respectively. Here the orthotropic material properties are considered, which can be implemented by maintaining geometrical symmetry along **X-Y** (2D cases) and **X-Y-Z** (3D cases) directions for all the microstructures. The predefined connectors for 2D and 3D microstructures to ensure the connectivity between two different microstructures are shown in Fig. 4.

In this study, unless otherwise specified, a total number of 11 discrete values after threshold are given to regularize the densities of finite elements at the macro scale, namely 0.001 (void), 0.1, 0.2, 0.3, 0.4, 0.5, 0.6, 0.7, 0.8, 0.9 and 1 (solid). It implies that only a total number of 9 representative microstructures with the intermediate densities need to be optimized in the concurrent design. The optimization terminates when the difference of the objective function between two successive iterations is less than 0.00001, or a maximum number of 300 iterations is reached.

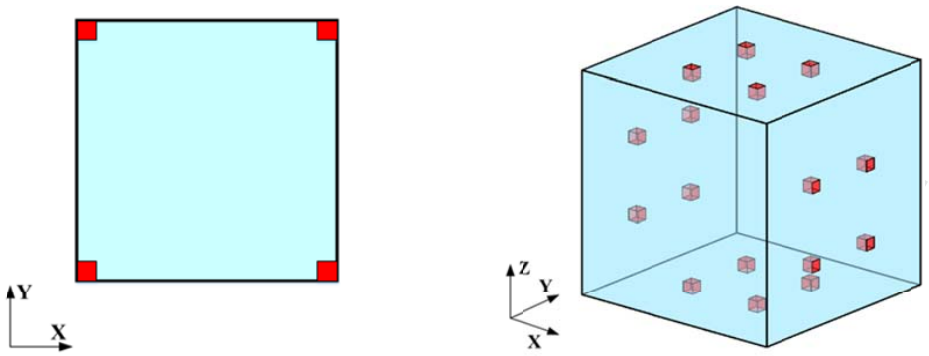

(a) (b)

Fig. 4. Predefined connectors (red squares or cubes) in microstructures: (a) 2D cases; (b) 3D cases.

5.1. Example 1

Fig. 5 shows a 2D cantilever beam with length L=120 and height H=40, undergoing a concentrated load P=5 at the center of the right edge. The macrostructure is discretized into 120×40=4800 elements with 4 nodes. The objective function is to minimize the structural compliance under a global volume constraint of 50%. As mentioned above, the local volume constraints for the 9 representative microstructures are 10%, 20%, 30%, 40%, 50%, 60%, 70%, 80% and 90%, respectively.

The multiscale concurrent design is shown in Fig. 6, including the topologically optimized macrostructure as well as the non-uniformly distributed microstructures with their optimal configurations. The right-side color bar shows the density of each macro finite element (or volume fraction of each microstructure), and different microstructures are plotted with different colors. The representative microstructures, as well as the properties and percentages for these microstructures in the optimized design are provided in Table 1. The iterative histories of the objective function and global volume constraint are given in Fig. 7. The iteration histories of the local volume constraints are plotted in Fig. 8.

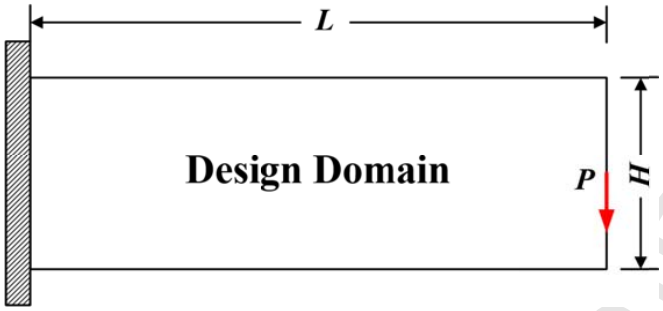

Fig. 5. Design domain of 2D cantilever beam

It can be seen from Fig. 6 that the external frame regions of the concurrent multiscale design is enhanced by a number of completely solids or high-density microstructures to bear loading and resist deformation, which complies with the well accepted topological design for the benchmark cantilever beam [4, 5, 67]. Here, the multiscale design contains a number of macro finite elements (or microstructures) with different intermediate densities. All the microstructures within the entire macrostructure are connected due to the setting of predefined connectors in different microstructures (Fig. 4(a)). As denoted in Table 1, the topologically designed microstructures after homogenization show orthotropic properties, which may result in better performances than the microstructures with isotropic properties in regards to the compliance optimization problem. The concurrent design can flexibly supply different directional stiffness, due to the different configurations of the representative microstructures. The final designs for all representative microstructures may have different topologies, shapes or sizes, but overall they are all featured with two crossed bars along the diagonal axes in each optimized design. Such structural skeletons (two crossed bars) for the microstructures well complies with the analytic design given in [68].

It should be noticed that only 9 types of representative microstructures are included in the final design. The macrostructure generally consists of several different types of multiple microstructural patches at some local regions, as indicated by different colors in Fig. 6. Each microstructural patch contains the identical microstructures. On one hand, from the aspect of computation, the total number of microstructures to be topologically designed is remarkably reduced when compared to the multiscale design with a large number of microstructures varying element-to-element. On the other hand, from the aspect of manufacturing, the optimized concurrent multiscale design is only characterized with a small limited number of representative

microstructures, rather than a great number of microstructures varying from element to element, which will greatly facilitate the subsequent manufacturing process even if the additive manufacturing is employed.

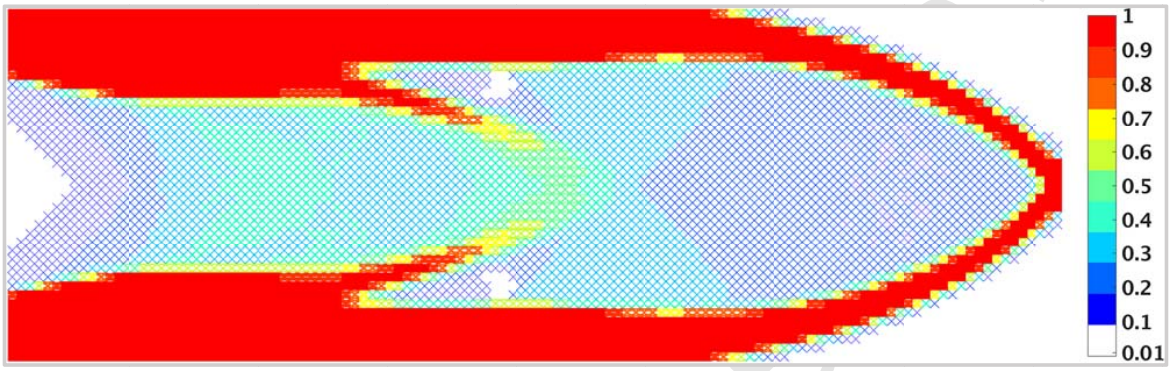

Fig. 6. Multiscale concurrent design of the cantilever beam with compliance 397.403

Fig. 7 shows that the macrostructural topology and the microstructural distributions keep being simultaneously optimized during the design process. It takes 108 steps for the concurrent optimization to converge to an optimal design. This reveals the powerful capability of the proposed method. It can be seen from Fig. 8 that the global volume constraint is conserved all the time, while the local volume constraints are satisfied gradually. The violation of local volume constraints during the earlier stage of the optimization accounts for the increase of the objective function at the first few iterations. After the base materials are gradually removed in all the microstructures to satisfy the local volume constraints, the structural compliance starts to reduce.

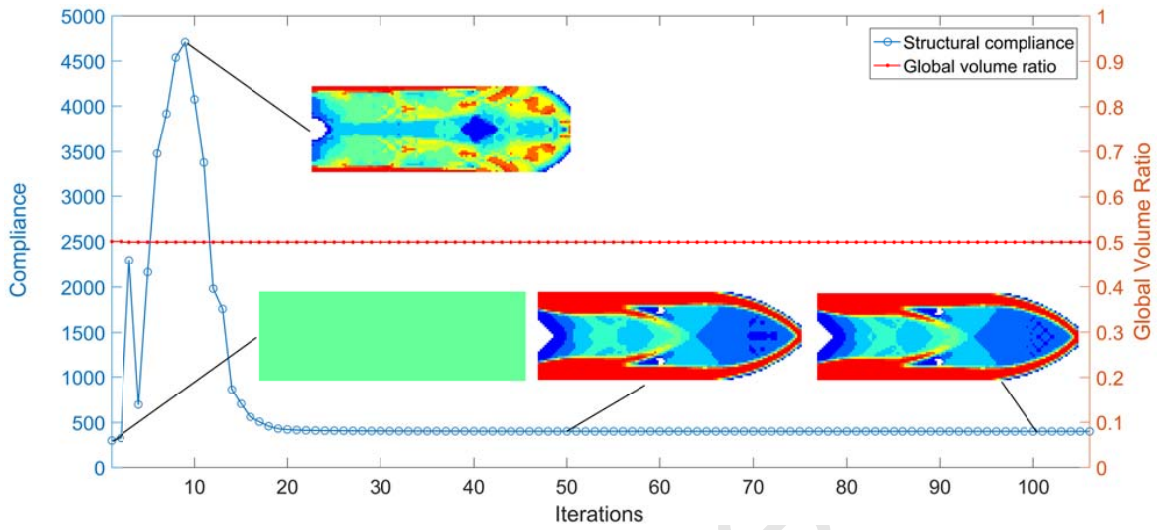

Fig. 7. Iterative histories of the objective function and global volume constraint

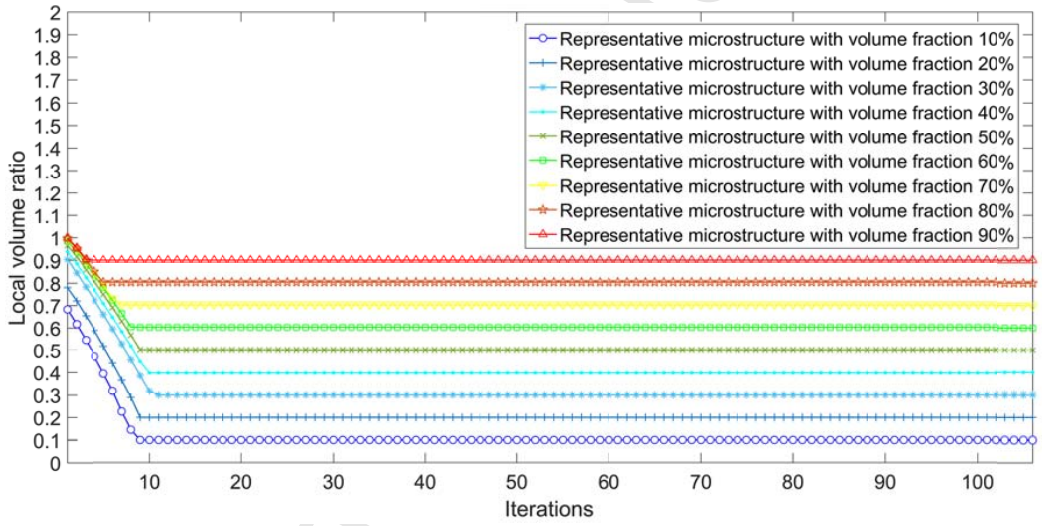

Fig. 8. Local volume constraints for the representative microstructures

To further show the benefits of the proposed multiscale concurrent design method, the optimized design is also compared with the conventional one-scale structure design, the one-scale homogeneous material microstructure design, as well as the multiscale concurrent design with uniformly distributed microstructures. Here, the one-scale designs refer to two different cases: structural design using the SIMP method [10]; and the homogeneous material microstructure design (without the topology changes of the macrostructure) also by using the SIMP method. The multiscale concurrent design with the uniform microstructures uses the same

design strategy discussed in [48], where the SIMP scheme is used at both scales. In the SIMP scheme, the penalty factor p=3 is adopted. For comparison, the FE models, the boundary conditions and the design domains in all the cases are the same, and the volume constraints (total material usages) for all designs are 50%.

Table 1. Representative microstructures and their corresponding properties

Volume fraction	Percentage	Microstructure	Level set	Property
10%	5.63%	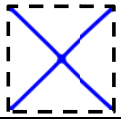	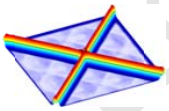	$\begin{bmatrix} 0.311 & 0.301 & 0 \\ 0.301 & 0.313 & 0 \\ 0 & 0 & 0.273 \end{bmatrix}$
20%	18.5%		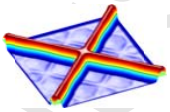	$\begin{bmatrix} 0.660 & 0.629 & 0 \\ 0.629 & 0.662 & 0 \\ 0 & 0 & 0.564 \end{bmatrix}$
30%	16.79%			$\begin{bmatrix} 1.090 & 1.003 & 0 \\ 1.003 & 1.103 & 0 \\ 0 & 0 & 0.860 \end{bmatrix}$
40%	8.58%		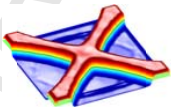	$\begin{bmatrix} 1.700 & 1.401 & 0 \\ 1.401 & 1.628 & 0 \\ 0 & 0 & 1.162 \end{bmatrix}$
50%	2.88%		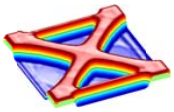	$\begin{bmatrix} 3.589 & 1.388 & 0 \\ 1.388 & 1.855 & 0 \\ 0 & 0 & 1.245 \end{bmatrix}$
60%	2.5%		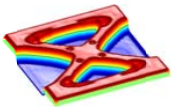	$\begin{bmatrix} 5.598 & 1.333 & 0 \\ 1.333 & 1.672 & 0 \\ 0 & 0 & 1.351 \end{bmatrix}$
70%	1.71%	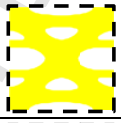	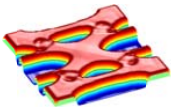	$\begin{bmatrix} 7.111 & 1.625 & 0 \\ 1.625 & 2.567 & 0 \\ 0 & 0 & 1.641 \end{bmatrix}$
80%	1.5%		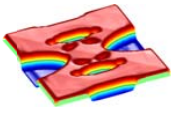	$\begin{bmatrix} 8.856 & 2.037 & 0 \\ 2.037 & 3.670 & 0 \\ 0 & 0 & 2.060 \end{bmatrix}$
90%	1.58%		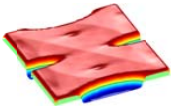	$\begin{bmatrix} 10.721 & 2.657 & 0 \\ 2.657 & 5.287 & 0 \\ 0 & 0 & 2.650 \end{bmatrix}$

(a) Macrostructural design using SIMP with compliance 409.746

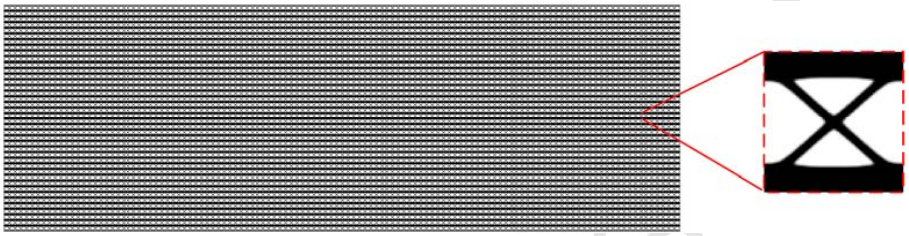

(b) Microstructural design using SIMP with compliance 853.979

Fig. 9. Designs by one-scale methods

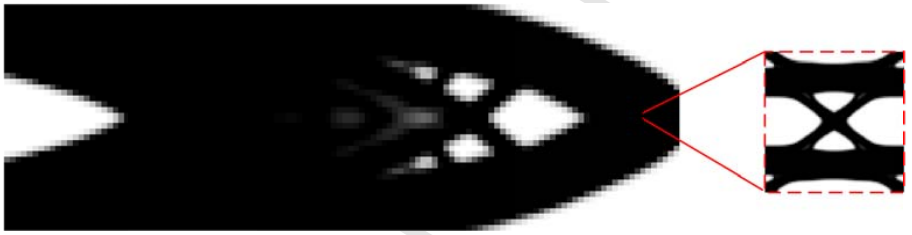

(a) Design (V_f^{MA}=83.3% and V_f^{MI}=60%) with compliance 714.081

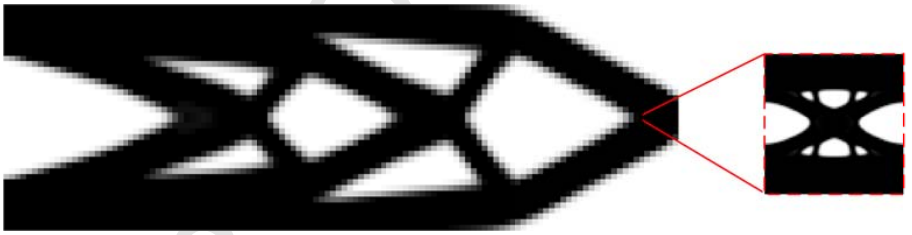

(b) Design (V_f^{MA}=62.5% and V_f^{MI}=80%) with compliance 550.035

Fig. 10. Multiscale concurrent designs with uniform microstructures

Fig. 9 shows the optimized designs obtained by both the one-scale structural and material design approaches, and Fig. 10 gives the optimized designs by the multiscale concurrent design with uniform microstructures. Figs. 10(a) and 10(b) are obtained by using different combinations of the macro volume constraint V_f^{MA} and the micro volume constraint V_f^{MI} [48, 50, 51], and the product of the two volume constraints at two scales are

both equal to 50%. It is noticed that the conventional one-scale macrostructural deign can achieve a better compliance than the one-scale material microstructure design, as well as the multiscale concurrent design having uniform microstructures. This observation is well in line with that in [48, 51, 54].

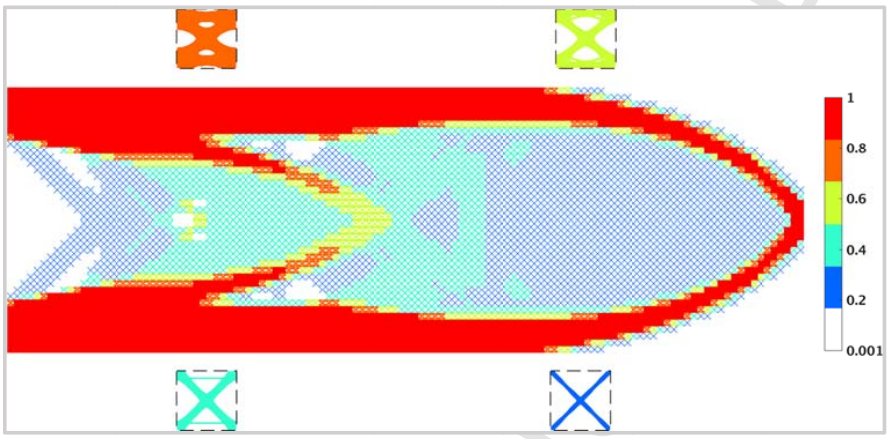

(a) 4 representative microstructures with compliance 401.474

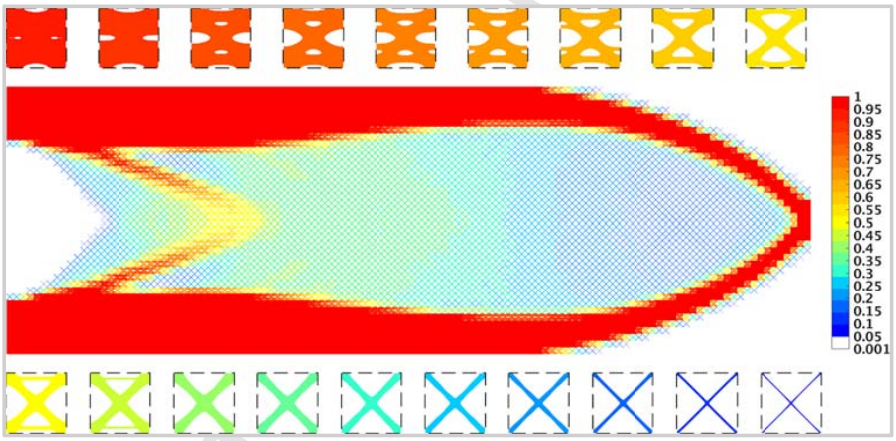

(b) 19 representative microstructures with compliance 396.785

Fig. 11. Multiscale designs with different number of representative microstructures

More importantly, for the concurrent design with uniform microstructures, its optimized design will have a higher compliance than the standard macrostructural topology design with solid materials in most of the compliance optimization problems [48, 51, 54]. However, in the proposed method, the multiscale concurrent design (Fig. 6) has the compliance lower than those of all the other designs given in Figs. 9 and 10, even lower than that of the standard macrostructural topology design with solid materials. The reason is that the proposed

method can greatly expand the multiscale design space by concurrently handling macrostructural topology layout, as well as the microstructural configurations and distributions. As a matter of fact, the current design in this study should belong to the heterogeneous cellular structures but with multiple patches of different homogeneous microstructures. Hence, it can be found that the proposed method can fully make use of different microstructures to maximize their abilities to bear loading in the concurrent design, and meanwhile maintain the computational efficiency and manufacturing easiness.

The concurrent designs achieved with different numbers of representative microstructures are also investigated. The multiscale concurrent design with 9 representative microstructures has already been given in Fig. 6, the designs with 4 and 19 representative microstructures are shown in Fig. 11. In these designs, the optimized representative microstructures are plotted besides the final multiscale concurrent designs, and different microstructures are indicated by using different colors (right-hand color bars). It can be seen that if more representative microstructures are included in the final design, a better structural compliance can be achieved. This is because more representative microstructures can enable a larger multiscale design space. However, it is easy to understand that too many representative microstructures will lead to more microstructures to be designed, and it will remarkably increase the computational cost.

5.2. Example 2

Fig. 12 shows a 2D Messerschmidt-Bölkow-Blohm (MBB) beam with length L=150 and height H=30. An external load P=5 is vertically applied at the center of the upper edge. The macrostructure is fixed at the bottom left corner, and its vertical degree of freedom with the bottom right corner is constrained. The 150×30=4500 elements with 4 nodes are used to discretize the macro design domain. The objective function is to minimize the structural compliance under several different global volume fraction constraints, namely 50%, 30% and 10%. Here a total number of 9 representative microstructures are used.

Normally, it is recognized that the one-scale macrostructural design can perform better than both the one-scale microstructure design and the multiscale concurrent design with uniform microstructures in most compliance optimization problems [48, 51, 54]. In this case, the multiscale concurrent designs obtained by

using the proposed method are compared with the one-scale macrostructural designs with the SIMP [10], under the same material usage constraints.

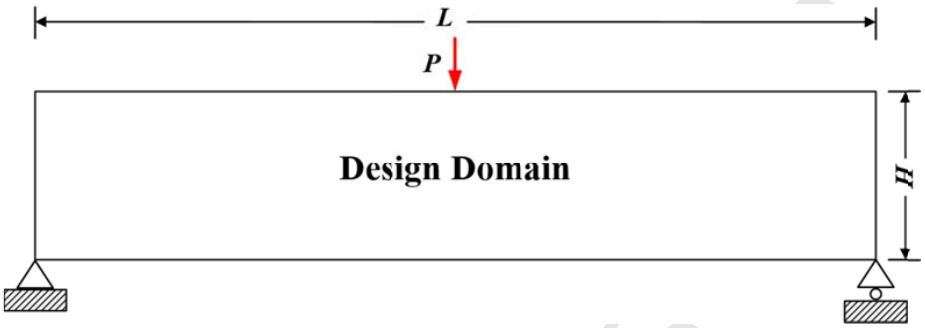

Fig. 12. Design domain of the 2D MBB beam

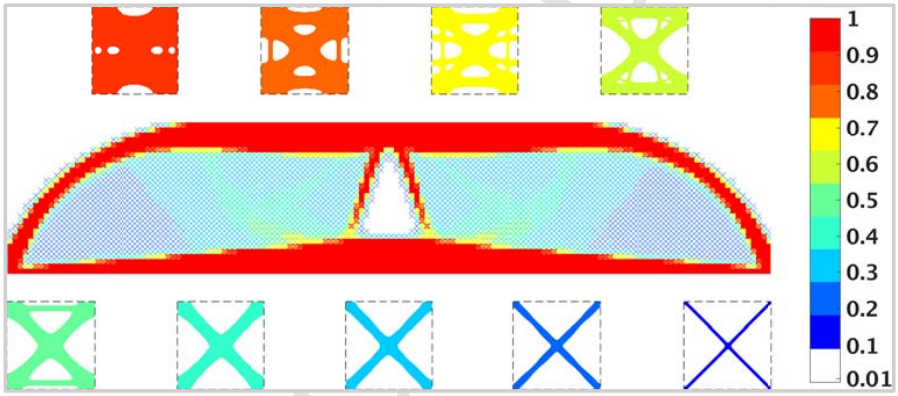

(a) Global volume fraction is 50%, compliance is 142.837

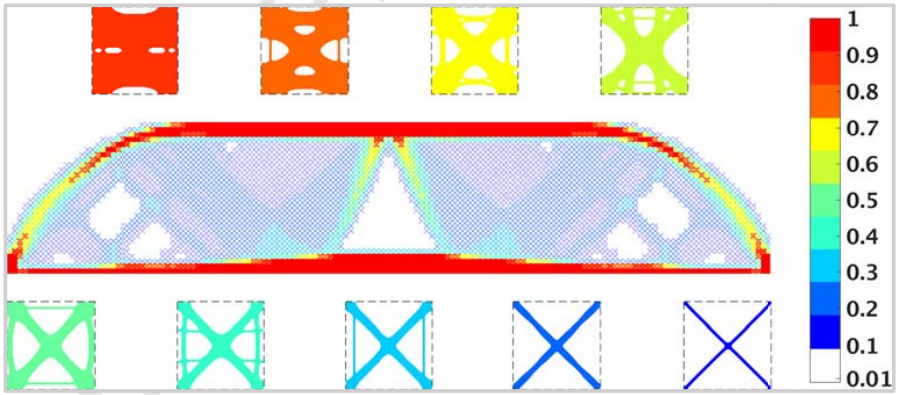

(b) Global volume fraction is 30%, compliance is 248.625

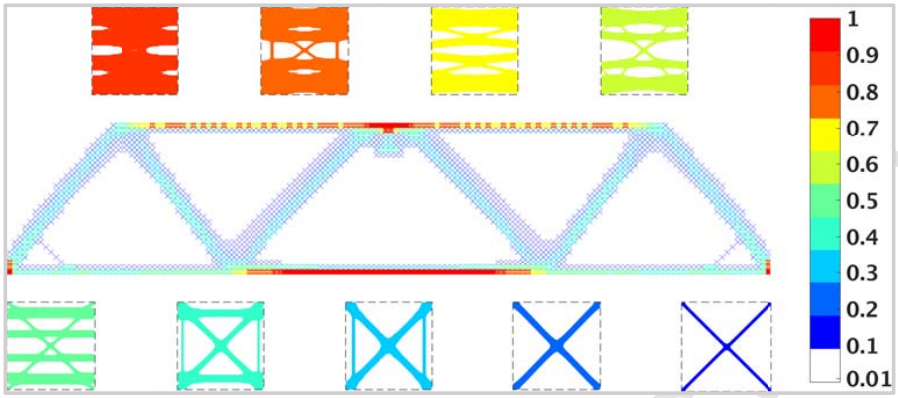

(c) Global volume fraction is 10%, compliance is 938.699

Fig. 13. Multiscale concurrent designs of the 2D MBB beam

The multiscale concurrent designs with different global volume fractions (i.e. overall material usages) by using the proposed method are given in Fig. 13. The one-scale macrostructural design results using the SIMP method under the corresponding volume fractions are given in Fig. 14. The optimized designs with the proposed method are connected in geometry due to the predefined connectors, as shown in Fig. 4(a). It is obvious that the multiscale concurrent designs in this paper have lower compliances than the macrostructure designs in all the numerical cases. It demonstrates the fact that the multiscale concurrent design method proposed in this paper can always broaden the design space, so as to achieve a better design performance.

It is of great interest to find that the multiscale concurrent design is obviously better than the conventional one-scale macrostructure design, when the overall allowable material usage is limited to 10%. The one-scale macrostructure optimization consumes over 1000 iterations. Under a relatively small volume constraint (e.g. 10%), the macrostructural optimization design in Fig. 14(c) is difficult to achieve a clear “black-white” design. However, the multiscale concurrent method can find an optimized design (see Fig. 14(c)) after 139 iterations, with clear and distinct structural topologies, which facilitate the manufacturability. It can be seen from Fig. 13(c) that the higher-density microstructures are mainly distributed at the upper and lower edges of the design, to enable the orthotropic properties with the clear material reinforcement orientation along the horizontal direction, so as to resist bending deformation for a long-span beam structure. This makes the entire structures more effective for transferring loads. Hence, the proposed design method can significantly improve the performance of the design, especially when the maximum material usage is at a low level.

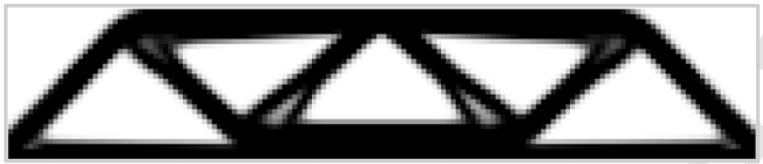

(a) Volume fraction is 50%, compliance is 148.951

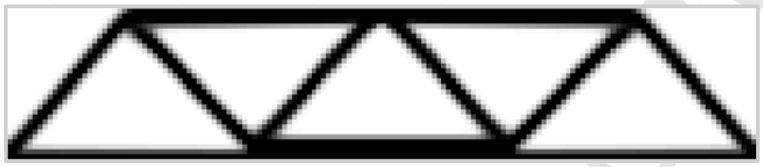

(b) Volume fraction is 30%, compliance is 253.808

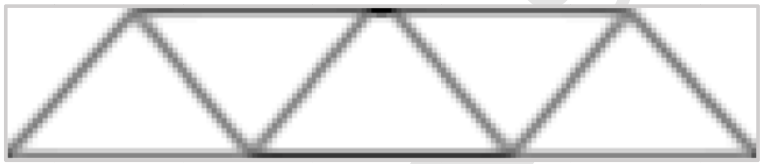

(c) Volume fraction is 10%, compliance is 2697.958

Fig. 14. One-scale macrostructure designs of the MBB beam

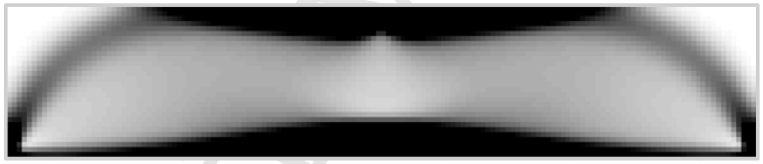

(a) Volume fraction is 50%, and compliance is 123.998

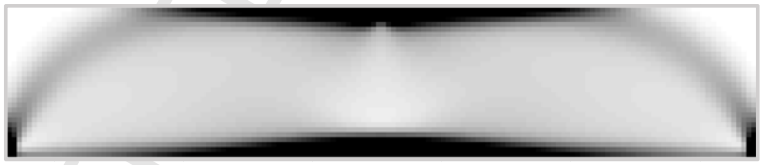

(b) Volume fraction is 30%, and compliance is 182.688

(c) Volume fraction is 10%, and compliance is 505.531

Fig. 15. Variable thickness sheet designs of the MBB beam

In particular, Fig. 15 provides the one-scale optimization designs by using the SIMP with p=1, namely the variable thickness sheet (VTS) method [4, 9, 67]. We can fund that the VTS designs are stiffer than the multiscale concurrent designs. On one hand, the limited types of representative microstructures and predefined connectors, used in the proposed concurrent design method to ensure the manufacturability, may restrict design flexibility in finding a higher-performance design. One the other hand, the close-walled cells (e.g. the variable thickness sheet designs) always perform better than the open-walled microstructures (e.g. the multiscale concurrent designs) under the same material volumes in the compliance design, due to the constraint of Hashin-Strikhman bounds on the porous microstructures [9, 67]. However, the VTS will result in designs with a great amount of thin sheets (grey elements) within the design domain, which may impose a significant challenge in fabrication. Furthermore, compare to the multiscale designs (Fig. 13), the VTS designs (Fig. 15) may give other difficulties in applications, e.g. stability, porosity, transparency or aesthetics [67]. Hence, the VTS method can achieve a stiffer design, but the multiscale concurrent design of cellular solids will provide more benefits when considering the diversity and flexibility in design, manufacturability and applications.

5.3. Example 3

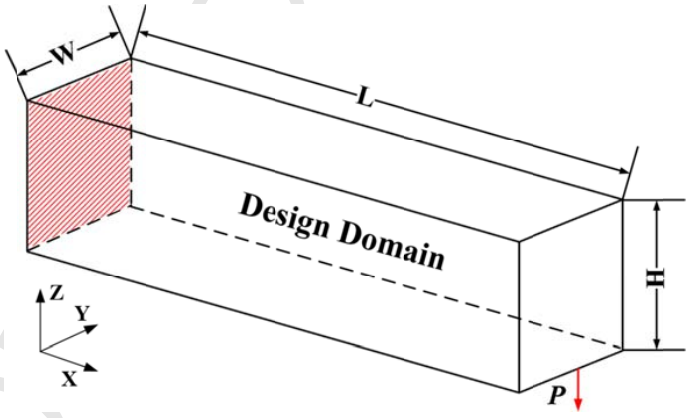

Fig. 16. Design domain of the 3D cantilever beam

A 3D cantilever beam with length L=40, width W=10 and height H=10 is given in Fig. 16. A concentrated load P=5 is vertically applied at the middle of the lower edge on the right end, and the left end is fixed. The macrostructure is discretized by using 40×10×10=4000 elements with 8 nodes. The objective function is to

minimize the structural compliance under the global volume fraction constraints of 30% and 10%, respectively. 9 representative microstructures are also considered in this example. For comparison, the SIMP-based macrostructure designs with the same volume fraction constraints are also provided.

The multiscale concurrent designs with different global volume fractions are plotted in Fig. 17, and the one-scale macrostructure designs with the same volume fractions are shown in Fig. 19. For a better visualization on the internal structures, the multiscale concurrent designs in Fig. 17 are further displayed with several masked microstructures, as shown in Fig. 18. For 3D structures, the designs obtained by using the proposed method also keep good connectivity in geometry. As shown in Figs. 17 and 18, at the macroscale, the higher-density elements are distributed along the upper and lower surfaces of the macrostructure, and the lower-density elements are mainly located at the region between the upper and lower faces. It makes sense for this kind of arrangement of the microstructures, which can better resist the deformation caused by the external load. The microstructures are reinforced and can produce directional stiffness mainly in the **X** and **Z** directions, as the major deformations of the entire structure are along these two directions. The similar topology layouts for microstructures have also been reported in a recent study [56].

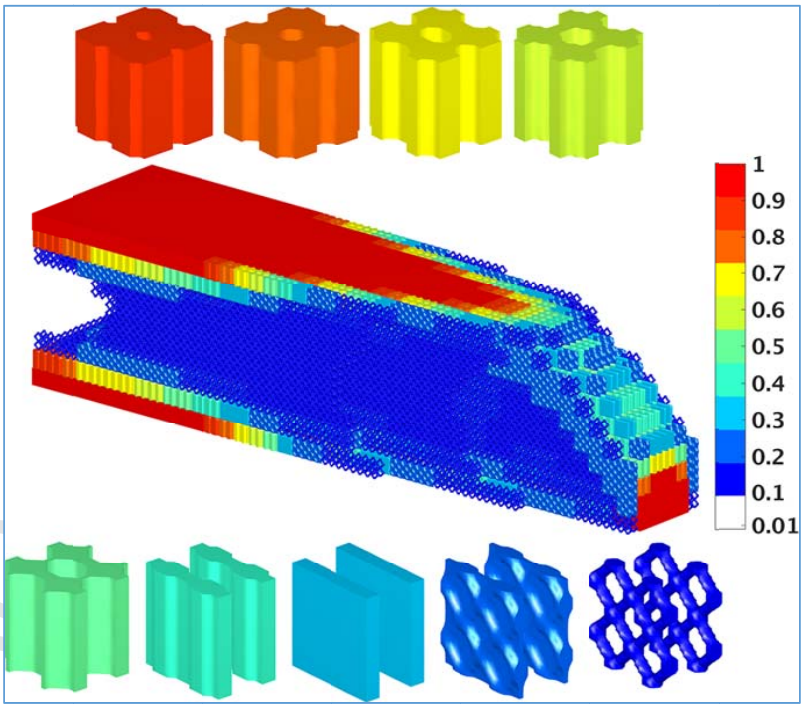

(a) Global volume fraction is 30%, compliance is 136.177

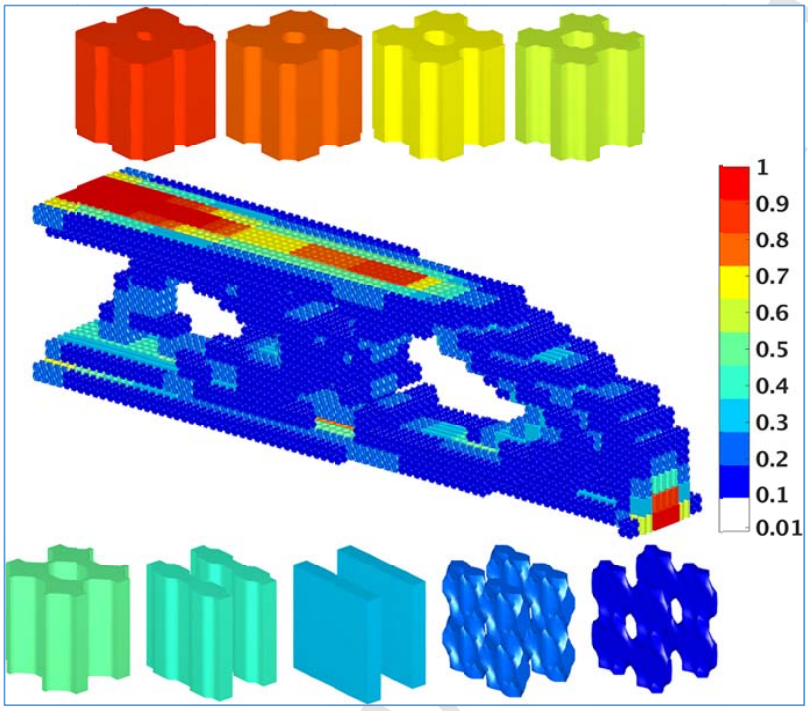

(b) Global volume fraction is 10%, compliance is 416.045

Fig. 17. Multiscale concurrent designs of the 3D cantilever beam

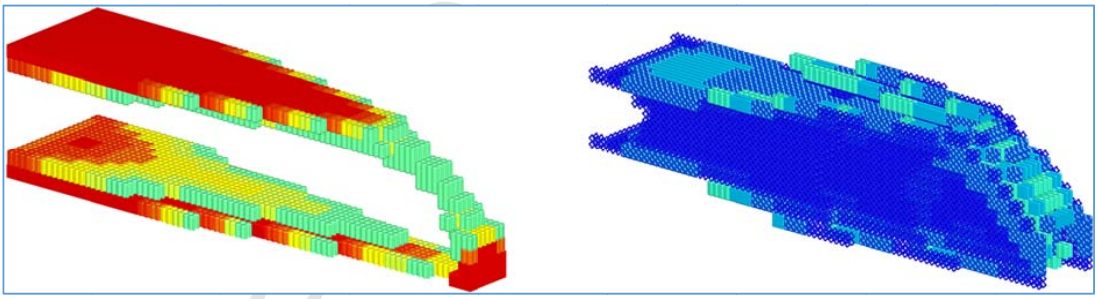

(a) 30% volume: mask lower-density microstructures (Left); mask higher-density microstructures (Right)

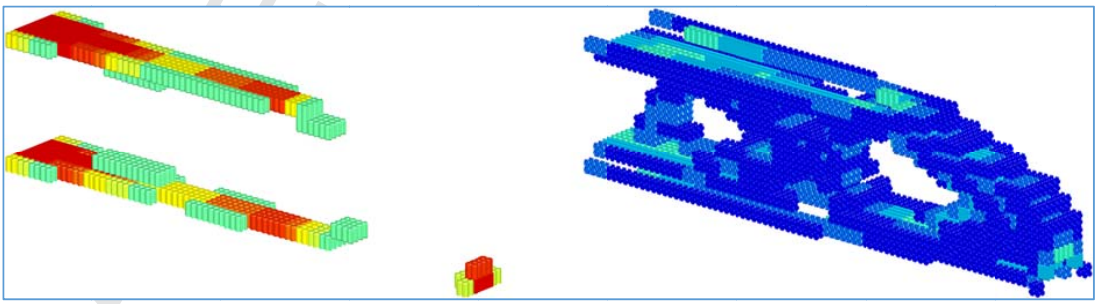

(b) 10% volume: mask lower-density microstructures (Left); mask higher-density microstructures (Right)

Fig. 18. Multiscale concurrent designs with masked microstructures

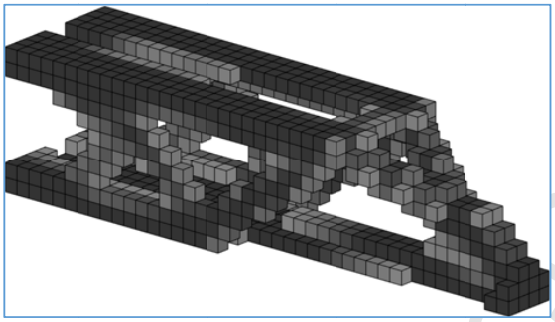

(a) Volume fraction is 30%, compliance is 206.544

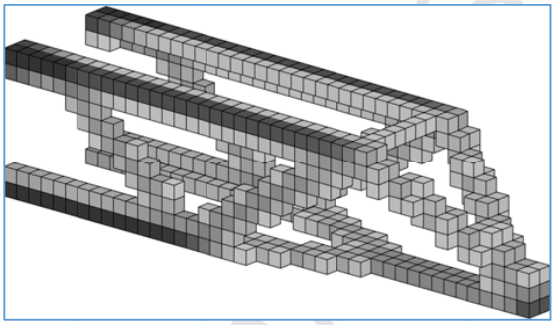

(b) Volume fraction is 10%, compliance is 1528.044

Fig. 19. One-scale macrostructure optimization designs of the 3D cantilever beam

From the above 3D numerical cases, it can be found that the multiscale concurrent design can produce much stiffer structures than the conventional one-scale macrostructural design. It is noticed that the improvement of the structural performance obtained by using the proposed multiscale design method for the 3D structure is more obvious than that of the 2D structure. The reason is that the design space of a 3D optimization problem is much larger than that of a 2D problem, and the proposed method can effectively explore the broader design space. This demonstrates the effectiveness of the proposed method for the design problems of 3D structures.

6. Conclusions

This paper has proposed a new multiscale concurrent topology optimization method for the design of heterogeneous cellular structures with non-uniformly distributed and multi-patch microstructures. In this method, both the macrostructural and microstructural topologies, as well as the distributions of microstructures are optimized simultaneously within a uniform optimization process. At the macro scale, a

discrete element density-based topology optimization method is developed to obtain the predefined discrete values for the design variables (macroscopic finite element densities). At the micro scale, all the macro finite elements with identical intermediate densities are represented by a representative microstructure with the same density (volume fraction). Thus, the types of different representative microstructures are determined according to the number of predefined discrete density values. The representative microstructures are topologically designed by using the PLSM together with the numerical homogenization method. Each individual representative microstructure is designed for all microstructures with the same volume fraction. Thus the total number of microstructures to be optimized is greatly reduced, and then the computational cost for the multiscale concurrent design is also considerably reduced. The numerical examples show that the proposed method can improve the structural performance, compared to the conventional one-scale structural design, the one-scale material design, as well as the multiscale concurrent design with uniform microstructures. The topologically designed heterogeneous cellular structures with a small number of homogeneous representative microstructures can greatly facilitate manufacturability. The proposed multiscale concurrent design method is actually general, and it can be extended to solve other design problems.

Acknowledgments

This research is partially supported by National Natural-Science-Foundation of China (51575204; 51705166), Australian Research Council (ARC) - Discovery Projects (160102491), National Basic Scientific Research Program of China (JCKY2016110C012), and China Postdoctoral Science Foundation (2017M612446).

References

[1] L.J. Gibson, M.F. Ashby, Cellular Solids: Structure and Properties, Cambridge University Press, Cambridge, 1997.
[2] R.M. Christensen, Mechanics of cellular and other low-density materials, Int. J. Solids Struct. 37 (2000) 93-104.
[3] S.C. Han, J.W. Lee, K. Kang, A new type of low density material: shellular, Adv. Mater. 27 (2015) 5506-5511.
[4] M.P. Bendsøe, O. Sigmund, Topology Optimization: Theory, Methods, and Applications, Springer, Berlin, Heidelberg, 2003.
[5] O. Sigmund, K. Maute, Topology optimization approaches: a comparative review, Struct. Multidiscip. Optim. 48 (2013) 1031-1055.

[6] M.P. Bendsøe, N. Kikuchi, Generating optimal topologies in structural design using a homogenization method, Comput. Methods Appl. Mech. Engrg. 71 (1988) 197-224.
[7] G. Allaire, Shape optimization by the homogenization method, Springer Verlag, New York, 2001.
[8] M. Zhou, G.I.N. Rozvany, The COC algorithm, part II: Topological, geometry and generalized shape optimization, Comput. Methods Appl. Mech. Engrg. 89 (1991) 309-336.
[9] M.P. Bendsøe, O. Sigmund, Material interpolation schemes in topology optimization, Arch. Appl. Mech. 69 (1999) 635-654.
[10] O. Sigmund, A 99 line topology optimization code written in Matlab, Struct. Multidiscip. Optim. 21 (2001) 120-127.
[11] Y.M. Xie, G.P. Steven, A simple evolutionary procedure for structural optimization, Comput. Struct. 49 (1993) 885-896.
[12] S. Osher, J.A. Sethian, Fronts propagating with curvature-dependent speed-algorithms based on Hamilton-Jacobi formulations, J. Comput. Phys. 79 (1988) 12-49.
[13] J.A. Sethian, A. Wiegmann, Structural boundary design via level set and immersed interface methods, J. Comput. Phys. 163 (2000) 489-528.
[14] M.Y. Wang, X.M. Wang, D.M. Guo, A level set method for structural topology optimization, Comput. Methods Appl. Mech. Engrg. 192 (2003) 227-246.
[15] G. Allaire, F. Jouve, A.M. Toader, Structural optimization using sensitivity analysis and a level-set method, J. Comput. Phys. 194 (2004) 363-393.
[16] G. Allaire, F. Jouve, A level-set method for vibration and multiple loads structural optimization, Comput. Methods Appl. Mech. Engrg. 194 (2004) 3269-3290.
[17] T. Belytschko, S.P. Xiao, C. Parimi, Topology optimization with implicitly function and regularization, Int. J. Numer. Methods Eng. 57 (2003) 1177-1196.
[18] Q. Xia, M.Y. Wang, S.Y. Wang, S.K. Chen, Semi-Lagrange method for level-set-based structural topology and shape optimization, Struct. Multidiscip. Optim. 31 (2006) 419-429.
[19] T. Yamada, K. Izui, S. Nishiwaki, A. Takezawa, A topology optimization method based on the level set method incorporating a fictitious interface energy, Comput. Methods Appl. Mech. Engrg. 199 (2010) 2876-2891.
[20] S. Yamasaki, S. Nishiwaki, T. Yamada, K. Izui, M. Yoshimura, A structural optimization method based on the level set method using a new geometry-based re-initialization scheme, Int. J. Numer. Methods Eng. 83 (2010) 1580-1624.
[21] N.P. van Dijk, M. Langelaar, F. van Keulen, Explicit level-set-based topology optimization using an exact Heaviside function and consistent sensitivity analysis, Int. J. Numer. Methods Eng. 91 (2012) 67-97.
[22] N.P. van Dijk, K. Maute, M. Langelaar, F. van Keulen, Level-set methods for structural topology optimization: a review, Struct. Multidiscip. Optim. 48 (2013) 437-472.
[23] P.D. Dunning, H.A. Kim, Introducing the sequential linear programming level-set method for topology optimization, Struct. Multidiscip. Optim. 51 (2015) 631-643.
[24] X. Guo, W. Zhang, W. Zhong, Explicit feature control in structural topology optimization via level set method, Comput. Methods Appl. Mech. Engrg. 272 (2014) 354-378.
[25] K. Svanberg, The method of moving asymptotes: a new method for structural optimization, Int. J. Numer. Methods Eng. 24 (1987) 359-373.
[26] S.Y. Wang, M.Y. Wang, Radial basis functions and level set method for structural topology optimization, Int. J. Numer. Methods Eng. 65 (2006) 2060-2090.

[27] Z. Luo, M.Y. Wang, S.Y. Wang, P. Wei, A level set-based parameterization method for structural shape and topology optimization, Int. J. Numer. Methods Eng. 76 (2008) 1-26.
[28] M.D. Buhmann, Radial Basis Functions: Theory and Implementations, Cambridge Monographs on Applied and Computational Mathematics, vol. 12, Cambridge University Press, New York, 2004.
[29] Y.Q. Wang, Z. Luo, N. Zhang, Z. Kang, Topological shape optimization of microstructural metamaterials using a level set method, Comput. Mater. Sci. 87 (2014) 178-186.
[30] H. Li, Z. Luo, N. Zhang, L. Gao, T. Brown, Integrated design of cellular composites using a level-set topology optimization method, Comput. Methods Appl. Mech. Engrg. 309 (2016) 453-475.
[31] Y. Wang, Z. Luo, N. Zhang, T. Wu, Topological design for mechanical metamaterials using a multiphase level set method, Struct. Multidiscip. Optim. 54 (2016) 937-952.
[32] H. Li, P.G. Li, L. Gao, L. Zhang, T. Wu, A level set method for topological shape optimization of 3D structures with extrusion constraints, Comput. Methods Appl. Mech. Engrg. 283 (2015) 615-635.
[33] J.L. Wu, Z. Luo, H. Li, N. Zhang, Level-set topology optimization for mechanical metamaterials under hybrid uncertainties, Comput. Methods Appl. Mech. Engrg. 319 (2017) 414-441.
[34] O. Sigmund, Materials with prescribed constitutive parameters: An inverse homogenization problem, Int. J. Solids Struct. 31 (1994) 2313-2329.
[35] O. Sigmund, A new class of extremal composites, J. Mech. Phys. Solids 48 (2000) 397-428.
[36] J.M. Guedes, N. Kikuchi, Preprocessing and postprocessing for materials based on the homogenization method with adaptive finite element methods, Comput. Methods Appl. Mech. Engrg. 83 (1990) 143-198.
[37] L. Xia, P. Breitkopf, Design of materials using topology optimization and energy-based homogenization approach in matlab, Struct. Multidiscip. Optim. 52 (2015) 1229-1241.
[38] O. Sigmund, S. Torquato, Composites with extremal thermal expansion coefficients, Appl. Phys. Lett. 69 (1996) 3203-3205.
[39] E. Andreassen, B.S. Lazarov, O. Sigmund, Design of manufacturable 3D extremal elastic microstructure, Mech. Mater. 69 (2014) 1-10.
[40] M.M. Neves, H. Rodrigues, J.M. Guedes, Optimal design of periodic linear elastic microstructures, Comput. Struct. 76 (2000) 421-429.
[41] J.K. Guest, J.H. Prévost, Optimizing multifunctional materials: Design of microstructures for maximized stiffness and fluid permeability, Int. J. Solids Struct. 43 (2006) 7028-7047.
[42] N. de Kruijf, S.W. Zhou, Q. Li, Y.W. Mai, Topological design of structures and composite materials with multiobjectives, Int. J. Solids Struct. 44 (2007) 7092-7109.
[43] S.W. Zhou, Q. Li, Design of graded two-phase microstructures for tailored elasticity gradients, J. Mater. Sci. 43 (2008) 5157-5167.
[44] A. Radman, X.D. Huang, Y.M. Xie, Topology optimization of functionally graded cellular materials, J. Mater. Sci. 48 (2013) 1503-1510.
[45] A. Faure, G. Michailidis, G. Parry, N. Vermaak, R. Estevez, Design of thermoelastic multi-material structures with graded interfaces using topology optimization, Struct. Multidiscip. Optim. (2017) online first.
[46] L. Xia, P. Breitkopf, Recent advances on topology optimization of multiscale nonlinear structures, Arch. Comput. Method Eng. 24 (2017) 227-249.
[47] D. Fujii, B.C. Chen, N. Kikuchi, Composite material design of two-dimensional structures using homogenization method, Int. J. Numer. Methods Eng. 50 (2001) 2031-2051.
[48] L. Liu, J. Yan, G.D. Cheng, Optimum structure with homogeneous optimum truss-like material, Comput. Struct. 86 (2008) 1417-1425.

[49] J. Yan, G.D. Cheng, L. Liu, A Uniform Optimum Material Based Model for Concurrent Optimization of Thermoelastic Structures and Materials, Int. J. Simul. Multidisci. Des. Optim. 2 (2009) 259-266.
[50] J.D. Deng, J. Yan, G.D. Cheng, Multi-objective concurrent topology optimization of thermoelastic structures composed of homogeneous porous material, Struct. Multidiscip. Optim. 47 (2013) 583-597.
[51] X.L. Yan, X.D. Huang, G.Y. Sun, Y.M. Xie, Two-scale optimal design of structures with thermal insulation materials, Compos. Struct. 120 (2015) 358-365.
[52] X. Guo, X.F. Zhao, W.S. Zhang, J. Yan, G.M. Sun, Multi-scale robust design and optimization considering load uncertainties, Comput. Methods Appl. Mech. Engrg. 283 (2015) 994-1009.
[53] W.M. Vicente, Z.H. Zuo, R. Pavanello, T.K.L. Calixto, R. Picelli, Y.M. Xie, Concurrent topology optimization for minimizing frequency responses of two-level hierarchical structures, Comput. Methods Appl. Mech. Engrg. 301 (2016) 116-136.
[54] J. Yan, X. Guo, G.D. Cheng, Multi-scale concurrent material and structural design under mechanical and thermal loads, Struct. Multidiscip. Optim. 57 (2016) 437-446.
[55] H. Rodrigues, J.M. Guedes, M.P. Bendsoe, Hierarchical optimization of material and structure, Struct. Multidiscip. Optim. 24 (2002) 1-10.
[56] P.G. Coelho, H.C. Rodrigues, Hierarchical topology optimization addressing material design constraints and application to sandwich-type structures, Struct. Multidiscip. Optim. 52 (2015) 91-104.
[57] W.H. Zhang, S.P. Sun, Scale-related topology optimization of cellular materials and structures, Int. J. Numer. Methods Eng. 68 (2006) 993-1011.
[58] F. Schury, M. Stingl, F. Wein, Efficient two-scale optimization of manufacturable graded structures, SIAM J. Sci. Comput. 34 (2012) B711-B733.
[59] L. Xia, P. Breitkopf, Concurrent topology optimization design of material and structure within FE^2 nonlinear multiscale analysis framework, Comput. Methods Appl. Mech. Engrg. 278 (2014) 524-542.
[60] R. Sivapuram, P.D. Dunning, H.A. Kim, Simutaneous material and structural optimization by multiscale topology optimization, Struct. Multidiscip. Optim. 54 (2016) 1267-1281.
[61] J. Ravnik, L. Škerget, M. Hriberšek, The wavelet transform for BEM computational fluid dynamics, Eng. Anal. Bound. Elem. 28 (2004) 1303-1314.
[62] E. Andreassen, C.S. Andreasen, How to determine composite material properties using numerical homogenization, Comput. Mater. Sci. 83 (2014) 488-495.
[63] K.K. Choi, N.H. Kim, Structural sensitivity analysis and optimization - linear systems, Springer, New York, 2005.
[64] J. Sokolowski, J.P. Zolesio, Introduction to shape optimization: shape sensitivity analysis, Springer, Berlin, 1992.
[65] J.E. Cadman, S.W. Zhou, Y.H. Chen, Q. Li, On design of multi-functional microstructural materials, J. Mater. Sci. 48 (2013) 51-66.
[66] J. Alexandersen, B.S. Lazarov, Topology optimisation of manufacturable microstructural details without length scale separation using a spectral coarse basis preconditioner, Comput. Methods Appl. Mech. Engrg. 290 (2015) 156-182.
[67] O. Sigmund, N. Aage, E. Andreassen, On the (non-)optimality of Michell structures, Struct. Multidiscip. Optim. 54 (2016) 361-373.
[68] G.I.N. Rozvany, O.M. Querin, J. Lógó, V. Pomezanski, Exact analytical theory of topology optimization with some pre-existing members or elements, Struct. Multidiscip. Optim. 31 (2006) 373-377.